Journal Pre-proof

The Development of Coronavirus 3C-Like Protease ($3CL^{pro}$) Inhibitors from 2010 to 2020

Yuzhi Liu, Chengyuan Liang, Liang Xin, Xiaodong Ren, Lei Tian, Xingke Ju, Han Li, Yongbo Wang, Qianqian Zhao, Hong Liu, Wenqiang Cao, Xiaolin Xie, Dezhu Zhang, Yu Wang, Yanlin Jian

PII: S0223-5234(20)30683-8

DOI: https://doi.org/10.1016/j.ejmech.2020.112711

Reference: EJMECH 112711

To appear in: *European Journal of Medicinal Chemistry*

Received Date: 22 June 2020

Revised Date: 17 July 2020

Accepted Date: 29 July 2020

Please cite this article as: Y. Liu, C. Liang, L. Xin, X. Ren, L. Tian, X. Ju, H. Li, Y. Wang, Q. Zhao, H. Liu, W. Cao, X. Xie, D. Zhang, Y. Wang, Y. Jian, The Development of Coronavirus 3C-Like Protease ($3CL^{pro}$) Inhibitors from 2010 to 2020, *European Journal of Medicinal Chemistry*, https://doi.org/10.1016/j.ejmech.2020.112711.

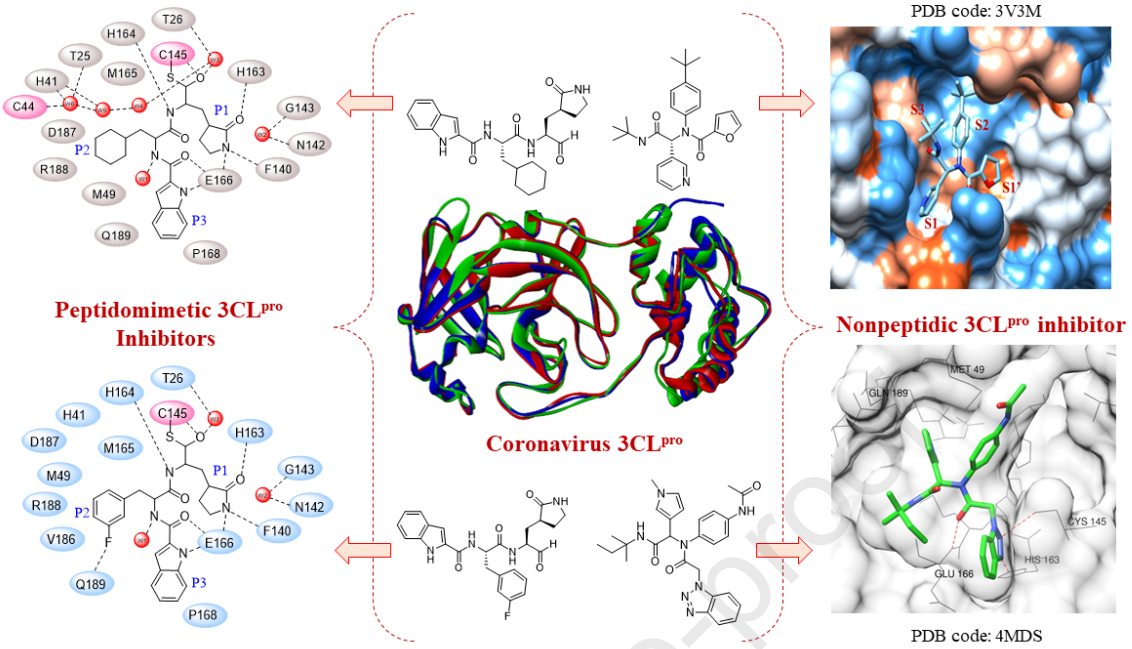

The Development of Coronavirus 3C-Like Protease ($3CL^{pro}$) Inhibitors from 2010 to 2020

Yuzhi Liu[1], Chengyuan Liang[1*], Liang Xin[1], Xiaodong Ren[2], Lei Tian[1], Xingke Ju[1], Han Li[1], Yongbo Wang[1], Qianqian Zhao[1], Hong Liu[3*], Wenqiang Cao[3], Xiaolin Xie[4], Dezhu Zhang[4],Yu Wang[4],Yanlin Jian[5*]

[1] Faculty of Pharmacy, Shaanxi University of Science & Technology, Xi'an 710021, P.R. China

[2] Medical College, Guizhou University, Guiyang 550025, P.R. China

[3] Zhuhai Jinan Selenium Source Nanotechnology Co., Ltd., Hengqin, Zhuhai, Guangdong, 519030, P.R. China

[4] Shaanxi Panlong Pharmaceutical Group Co., Ltd., Xi'an 710025, P.R. China

[5] Laboratory for Medicinal Chemistry (FFW), Ghent University, Ottergemsesteenweg 460, B9000, Gent, Belgium

* Correspondence:

chengyuanliang@gmail.com (C.L.); sesource_liuhong@163.com(H.L.); yanlin.jian@ugent.be (Y.J.)

Contents

1. Introduction 2

1.1 COVID-19 pandemic 2

1.2 Coronaviruses and their therapeutic targets 3

2. 3CL protease 3

3. Peptidomimetic $3CL^{pro}$ inhibitors 4

4. Nonpeptidic $3CL^{pro}$ inhibitor 7

4.1 Decahydroisoquinoline and octahydro-isochromene derivatives 7

4.2 $3CL^{pro}$ inhibitor with a 3-pyridyl or triazole moiety 9

4.3 $3CL^{pro}$ inhibitor with a piperidine moiety 12

4.4 Unsymmetrical aromatic disulphides 13

4.5 Serine derivatives 13

4.6 Pyrazolone and pyrimidines 15

4.7 Natural product derivatives 16

4.7.1 Flavonoids, biflavonoids and chalcones 16

4.7.2 Isatin derivatives 17

4.7.3 Terpenoid derivatives 17

5. Discussion and perspectives 18

Acknowledgements 21

References 22

Abstract

$3CL^{pro}$ is a key enzyme for the maturation of all coronaviruses and has hence been recognized as a potent drug target for the treatment of coronavirus infection. The present review focuses on the status of various efficacious anti-coronavirus small-molecule inhibitors found from various sources in the past 10 years (2010-2020) and describes in detail the structural characteristics, binding modes and SARs of these $3CL^{pro}$ inhibitors. To solve the shortcomings of "off-target" side effects and weak inhibitory activity of existing $3CL^{pro}$ inhibitors, the authors propose a new idea for drug design, combining the emerging PROTAC technology with existing $3CL^{pro}$ inhibitors. $3CL^{pro}$ PROTAC degraders are proposed as the next generation of anti-coronavirus drugs.

Keywords

Coronaviruses, 3C-Like Protease ($3CL^{pro}$) Inhibitors, Peptidomimetic Inhibitors, COVID-19, Proteolysis-Targeting Chimaera (PROTAC).

1. Introduction

1.1 COVID-19 pandemic

Coronavirus disease 2019 (COVID-19) is a highly infectious disease caused by severe acute respiratory syndrome coronavirus 2 (SARS-CoV-2), a virus that is closely related to the SARS virus [1]. As of July 10, 2020, the COVID-19 pandemic had spread to 212 countries, and more than 10 million people had been diagnosed with the infection worldwide [2, 3]. SARS-CoV-2 primarily spreads via small droplets expelled by infected individuals when they breathe or cough [4, 5]. Infected individuals may either be asymptomatic or develop common COVID-19 symptoms, including fever, cough, fatigue, shortness of breath, and loss of smell [6], and severe

cases can progress to complications, including pneumonia, acute respiratory distress syndrome, multi-organ failure, and death [7].

1.2 Coronaviruses and their therapeutic targets

Coronaviruses are species of viruses belonging to the subfamily *Orthocoronavirinae* in the family *Coronaviridae* of the order *Nidovirales*. Coronaviruses are single-stranded positive-sense RNA viruses [8, 9] that are endowed with the largest viral genomes (27-32 kb) among the RNA viruses identified to date [10]. Before SARS-CoV-2, six coronaviruses were found to infect humans: human coronavirus (HCoV)-229E, HCoV-OC43, HCoV-NL63, HCoV-HKU1, SARS-CoV and Middle East respiratory syndrome coronavirus (MERS-CoV). The first four are constrained endemic strains that cause the common cold, whereas the latter two can cause severe respiratory epidemics [11-13]. Based on their high prevalence and widespread distribution, as well as their genetic diversity and the frequent recombination of the genome, coronaviruses pose a constant threat to humans [14-16].

At present, potential therapeutic targets for coronaviruses can be divided into structural proteins and nonstructural proteins (nsps). Structural proteins mainly include the spike protein (S) [17, 18], envelope protein (E), nucleocapsid phosphoprotein (N) and membrane protein (M) [19]. Nsps mainly include 3C-like protease ($3CL^{pro}$), papain-like protease (PL^{pro}), RNA-dependent RNA polymerase (RdRp, nsp12) [20], RNA helicases (nsp13), guanine-N7 methyltransferase (nsp14), and uridylate-specific endoribonuclease (nsp15) [21, 22]. An additional target is angiotensin-converting enzyme 2 (ACE2) [22, 23]. Among these targets, $3CL^{pro}$ plays an important role in the process of virus replication and is of value, and studies have found that the SARS-CoV-2 $3CL^{pro}$ sequence is highly homologous to those of coronaviruses such as SARS-CoV and MERS-CoV.

2. 3CL protease

The coronavirus $3CL^{pro}$ is a cysteine protease composed of approximately 300 amino acids [24, 25]. $3CL^{pro}$ can cut and functionalize the two polyproteins pp1a and pp1ab, which are translated from the first open reading frame (ORF 1a/b) of the

coronavirus, to yield 16 nsps (**Fig 1**) [26, 27]. $3CL^{pro}$ contains three domains [28, 29], including a non-classical Cys-His catalytic dyad (Cys145 and His41) in the gap between domains I and II [30]; can specifically recognize the 11 cleavage sites of nsp4~nsp16; and exhibits self-hydrolytic cleavage activity [31, 32]. These functional nsps (nsp4~nsp16) released by cleavage with $3CL^{pro}$ are responsible for viral genome replication and transcription, and nsp4~nsp16 also play roles in other important viral life processes, such as protein translation, cleavage, and modification and nucleic acid synthesis [25, 33]. Therefore, inhibition of $3CL^{pro}$ can effectively block viral RNA replication and transcription and further block viral proliferation.

Fig 1.

In addition, $3CL^{pro}$ is highly conserved among the known coronavirus species, and several common features are shared among the different coronavirus $3CL^{pro}$ substrates. From the N terminus to the C terminus, the amino acids in the substrates are numbered -P4-P3-P2-P1↓P1'-P2'-P3'-, and the cleavage site is located between P1 and P1' [34, 35]. In particular, a Gln residue is almost always required at the P1 position of the substrates. Nevertheless, amino acid sequence alignments indicate that the similarity of the $3CL^{pro}$ of SARS-CoV-2 and SARS-CoV can be as high as 96.1% [36, 37]. Only 12 of the 306 residues differ, namely, T35V, A46S, S65N, L86V, R88K, S94A, H134F, K180N, L202V, A267S, T285A and I286L, and these different amino acid residues are $3CL^{pro}$ inactive sites [38, 39]. Further sequence comparisons have revealed that the $3CL^{pro}$ of the three coronaviruses SARS-CoV-2, SARS-CoV, and MERS-CoV exhibit a high degree of structural similarity and conservation **(Fig 2)** [40]. These findings indicate that $3CL^{pro}$ could be used as a homologous target for the development of anti-coronavirus drugs that can inhibit the proliferation of various coronaviruses.

Fig 2.

3. Peptidomimetic $3CL^{pro}$ inhibitors

Structurally, $3CL^{pro}$ inhibitors can be classified as peptoids and nonpeptidomimetics, and the mechanism of action of peptide inhibitors includes two

steps. Peptidomimetics that mimic natural peptide substrates initially bind to $3CL^{pro}$ and form a noncovalent complex, and the warhead group, which is spatially very close to the catalytic residue of the target protein, undergoes nucleophilic attack to catalyse the formation of covalent bonds involving cystein [41, 42]. These warheads mainly contain Michael receptors [43, 44], aldehydes [45] and different types of ketones (see **Fig 3** and **Table 1**) [46-48], which covalently bind to the Cys145 residue in the $3CL^{pro}$ S1' pocket to exert an inhibitory effect.

Table 1 Peptidomimetic $3CL^{pro}$ inhibitors

Type	Categories	Compound No.	Ref.
1	Michael acceptor peptidomimetics	1-6	[49-51]
2	Aldehyde peptidomimetics	7-12	[51]
3	**Keto peptidomimetics**	**13-27**	[47]
3-1	Fluoromethyl ketone	13-18	[52]
3-2	1,4-Phthalazinedione	19-20	[53]
3-3	Benzothiazolone	21-23	[54, 55]
3-4	α-Ketoamide	24-27	[56]

Fig 3.

Among these peptidomimetic inhibitors, aldehyde compounds **11** and **12** and α-ketoamide compounds **25-27** showed good inhibitory activity against the current SARS-CoV-2. Compounds, which are novel inhibitors designed and synthesized for SARS-CoV-2 $3CL^{pro}$ by Hong Liu and colleagues [57], exhibit excellent inhibitory activity against SARS-CoV-2 $3CL^{pro}$ (**11**: IC_{50}=0.053±0.005 μM, **12**: IC_{50}=0.040±0.002 μM). Moreover, *in vitro* antiviral activity assays have indicated that compounds **11** and **12** exert potent anti-SARS-CoV-2 effects, with EC_{50} values of 0.53 μM and 0.72 μM, respectively, and both exhibit good *in vivo* pharmacokinetic (PK) properties and an acceptable preliminary safety profile and have the potential to be new anti-SARS-CoV-2 preclinical candidates. Based on an analysis of the substrate-binding pocket of SARS-CoV $3CL^{pro}$ (PDB code: 2H2Z), an aldehyde was selected as the warhead in P1 that would form a covalent bond with cysteine. A

detailed diagram of the interaction between compound **11** and SARS-CoV-2 $3CL^{pro}$ shows that the aldehyde carbonyl of **11** and the catalytic site Cys145 of SARS-CoV-2 $3CL^{pro}$ form a standard C-S covalent bond (**Fig 4-A**). The oxygen atom of the aldehyde group forms a hydrogen bond with the backbone of the Cys145 residue at the S1' site, which is crucial for stabilizing the binding conformation. The (*S*)-γ-lactam ring at P1 is compatible with the S1 site, and the oxygen atom of the (*S*)-γ-lactam group forms a hydrogen bond with the His163 side chain, the main chain of Phe140 and the side chain of Glu166 and forms a hydrogen bond with the NH group of the (*S*)-γ-lactam ring. The cyclohexyl part at the P2 position can be inserted into the S2 position and stacks with the imidazole ring of His41. The indole group at the P3 position is exposed to the solvent (S4 site) and forms a hydrogen bond with Glu166. Interestingly, multiple water molecules (named W1-W6) play important roles in the binding of **11**: W1 interacts with the amide bond of **11** through hydrogen bonding, whereas W2-W6 forms a few hydrogen bonds with the aldehyde group of **11** and the residues Asn142, Gly143, Thr26, Thr25, His41 and Cys44, which contribute to the stability of the binding pocket of **11**. The binding mode of compound **12** is very similar to that of **11** (**Fig 4-B**). The difference in their binding modes might be due to the 3-fluorophenyl at the P2 position of compound **12**. The side chains of the residues His41, Met49, Met165, Val186, Asp187 and Arg188 interact with the aryl group through hydrophobic interactions, and the side chain of Gln189 stabilizes 3-fluorophenyl via additional hydrogen bonding.

Fig 4.

Rolf Hilgenfeld et al. previously revealed that the peptidomimetic α-ketoamide inhibitor **24** serves as a broad-spectrum inhibitor of the 3CLpro of β-coronaviruses, α-coronaviruses and enteroviruses [56]. Compound **24** exhibits a low EC_{50} for SARS-CoV and a number of enteroviruses in different cell lines (EC_{50}<5 μM); notably, the EC_{50} of MERS-CoV in Huh7 cells is 400 pM. Lead **24** has been subjected to various structural modifications [58]. To improve its half-life in plasma, compound **24** was modified by shielding the P3-P2 amide bond on the pyridone ring (**Fig 5**, green circle), which is expected to prevent off-target contacts and the cleavage of this

bond by other cellular proteases. In addition, to enhance the solubility of **24** in plasma, the hydrophobic cinnamyl was replaced by a low-hydrophobicity Boc group (**Fig 5**, red circle), which produced **25**. Moreover, the cyclohexyl at P2 of **25** was substituted with the smaller cyclopropyl (**Fig 5**, blue circle) to render **26**, which might show enhanced antiviral activity against the β-coronaviruses of clade b (SARS-CoV-2 and SARS-CoV). However, compound **27**, which was obtained by removal of the Boc group of **26**, was almost inactive (**Fig 5**, purple circle), which indicated that the hydrophobic group is necessary for crossing the cell membrane and binding to viral $3CL^{pro}$. A PK study demonstrated that 4 hours after subcutaneous administration, the lung tissue concentration of **26** was approximately 13 ng/g. The lung tropism of **26** was a favourable target organ aggregation characteristic because COVID-19 and other coronaviruses mostly affect lung tissue. As a complementary route of administration, **26** can also be nebulized with an inhalation device at 3 mg/kg. Even 24 hours after administration, the concentration of **26** in lung tissue remained at 33 ng/g. A mouse lung drug inhalation model showed that **26** is well tolerated without adverse reactions, which indicates that inhalers might be a suitable method for administration of **26**. The other peptidomimetic inhibitors shown in **Fig 3** and **Table 1** were described in detail in a previous review by Thanigaimalai Pillaiyar et al. [59].

Fig 5.

4. Nonpeptidic $3CL^{pro}$ inhibitor

4.1 Decahydroisoquinoline and octahydro-isochromene derivatives

Fig 6.

Inspired by the interaction of peptide inhibitor **28** between S1 and S2 of SARS-CoV $3CL^{pro}$, Shimamoto Yasuhiro et al. [60] designed and synthesized a series of competitive SARS-CoV $3CL^{pro}$ inhibitors (compounds **29a**-**29d**, **Fig 6**) with a decahydroisoquinoline fused ring scaffold. All synthetic decahydroquinoline inhibitors exhibited moderate to significant inhibition of SARS $3CL^{pro}$. According to X-ray crystallography (PDB code: 4TWY, **Fig 7**), the fused ring structure of dehydroquinoline occupies most of the space in the S2 pocket. X-ray crystallography

analyses have confirmed that the decahydroisoquinoline inhibitor is located in the fissure of the active centre of $3CL^{pro}$, similar to the results obtained with the high-efficiency peptide-aldehyde lead compound. The decahydroisoquinoline scaffold was inserted into a large S2 pocket and filled most of the pocket space. As expected, the imidazole at the P1 site was inserted into the S1 pocket. These interactions effectively fixed the terminal aldehyde in the fissure of the active centre, and the new scaffold thus closely fit into the $3CL^{pro}$. Acyl groups on nitrogen atoms in decahydroisoquinoline scaffolds are located on the surface of $3CL^{pro}$, where additional interactions might occur with $3CL^{pro}$. These interactions effectively fixed the terminal aldehyde tightly at the active site, resulting in a novel decahydroquinoline scaffold that cooperates closely with $3CL^{pro}$. To evaluate the effect of the configuration on the dehydroisoquinoline scaffold, the IC_{50} values of trans-decahydroisoquinolin diastereomers in *N*-4-phenylbenzoyl derivatives (**29a** vs **29b**) or *N*-4-bromo benzoyl derivatives (**29c** vs **29d**) were compared, and the results clearly showed that the (4a*R*, 8a*S*) isomer is more potent than the (4a*S*, 8a*R*) isomer.

Fig 7.

Based on the abovementioned findings, Shimamoto Yasuhiro et al. performed further structural modification, and an octahydro-isochromene scaffold was selected as a new type of hydrophobic fused ring (**Fig 8**). An alkyl or aryl substituent was also introduced at the 1-position of the octahydro-isochromene scaffold. The effects of the configuration of the fused ring structure and those of various substituents on the inhibition of SARS $3CL^{pro}$ were evaluated. Sharpless-Katsuki asymmetric epoxidation and Sharpless asymmetric dihydroxylation were employed to synthesize the octahydro-isochromene moiety. Introduction of (*S*)-2-amino-3-imidazolyl propanal (His-al) at the P1 site and the substituent at the 1-position was achieved through successive reductive amination reactions. *N*-butyl (**30**), isobutyl (**31**), allyl (**32**) and benzyl (**33**) were introduced at the 1-position, and the IC_{50} value for SARS $3CL^{pro}$ indicates that the n-butyl substituent is expected to undergo a certain interaction with the protease. The stereochemical effect of the octahydro-isochromene scaffold was also investigated, and the results showed that the specific (1*S*, 3*S*) configuration of **35**

can orient imidazole and the warhead aldehyde at the P1 site to the corresponding $3CL^{pro}$ pockets [61].

Fig 8.

Additionally, Kouji Ohnishi et al. [62] introduced a nonprime site substituent at the 4-position carbon of the decahydroisoquinolin skeleton to yield the nonpeptidic inhibitor **38**, which exhibits moderate but enhanced inhibitory activity against R188I SARS $3CL^{pro}$ (IC_{50}=26 μM). The results indicated significantly increased affinity between **38** and SARS $3CL^{pro}$ at the S3 to S4 pockets.

Fig 9.

4.2 $3CL^{pro}$ inhibitor with a 3-pyridyl or triazole moiety

Fig 10.

Jacobs et al. [42] conducted a high-throughput screening of National Institute of Health (NIH) molecular libraries (approximately 293,000 compounds) to find hits for $3CL^{pro}$ inhibitors. The analysis of a dipeptide compound library identified **39** (**Fig 10-A**), which had an IC_{50} less than 10 μM and was thus considered an exceptionally good candidate. Thus, a series of 3-pyridyl derivatives were subsequently optimized based on hit **39**, and the resulting compounds **40a** (IC_{50}=2.2 μM) and **40b** (IC_{50}=2.1 μM) exhibited compelling inhibitory activity against SARS-CoV $3CL^{pro}$. The X-ray crystal structure of ***(R)*-40a** combined with SARS-CoV $3CL^{pro}$ (**Fig 11**) demonstrated that ***(R)*-40a** preferentially occupied the S1'-S3 $3CL^{pro}$ subpockets. According to the identified binding mode, the tert-butyl amide occupies the S3 pocket, the tert-butyl anilido group occupies a deep S2 pocket, and the 3-pyridyl group occupies the S1 pocket.

Fig 11.

To further clarify the structure-activity relationship (SAR) of lead compound **40a**, the P1-P3 framework was maintained consistently, while a library of five-membered aromatic heterocycles was synthesized through alterations in the P1' position (**Table 2, 41a-41f**). Among the resulting compounds, imidazole-substituted (**41c**, IC_{50}=6 μM) and 5-chlorofuran-substituted (**41e**, IC_{50}=5.2 μM) analogues were found to be the most potent. A subsequent study of P1 replacements was performed to identify

alternative hydrogen bond acceptor groups that might engage His163 while retaining the 2-furyl amide P1' group. Among the six-membered π-excessive heterocycles examined (**42a-42c**), pyridazine (**42a**) and pyrazine (**42b**) were well tolerated. Furthermore, chiral stationary-phase supercritical fluid chromatography (SFC) was applied to separate **40a** enantiomers (**Fig 10-B**), and highly specific inhibition was obtained with the single stereoisomer **(*R*)-40a (ML188),** which exhibited an IC_{50} of 1.5±0.3 μM.

Table 2 Variation at the P1' (**41a-41f**) and P1(**42a-42c**) sites of **40a** (*R&S*)

	Compound	**P1'**	**3CL^{pro} IC_{50} (μM)**		**Compound**	**P1**	**3CL^{pro} IC_{50} (μM)**
	41a		39		**42a**		10
	41b		50		**42b**		5.5
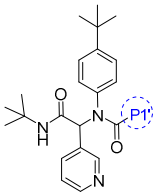	**41c**		6	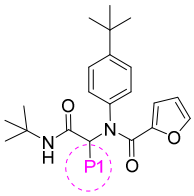	**42c**		45
	41d		47				
41	**41e**	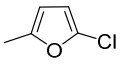	5.2	**42**			
	41f		75				

Further screening revealed that a class of noncovalent benzotriazole inhibitors from the NIH Molecular Libraries Probe Production Centers Network (MLPCN) exhibited improved biological activity [63]. Among these compounds, compound **43**

substantially inhibited SARS-CoV $3CL^{pro}$ (IC_{50}=6.2 μM).

According to X-ray crystallography (PDB code: 4MDS, **Fig 12**), rearrangement of the Gln189 and Met49 residue side chains forms the diamide **43**, which exhibits an induced-fit binding site. This induced-fit binding site accommodates the *syn N*-methyl pyrrole and anilido acetamide moieties of the inhibitors within the S2-S4 and S2-S1' subpockets, respectively. In addition to the P2-P4 and P2-P1' groups, **43** partially occupies the S3 subpocket with a terminating 2-methylbutylamide. Moreover, Cys145 and benzotriazole N-(2) form a key hydrogen bond near the catalytic centre. Other hydrogen bond interactions are found near the catalytic site of His163 and benzotriazole N-(3), and the main chain Glu-166 NH shows an obvious interaction with the central acetamide oxide.

Fig 12.

As a promising hit, the template compound **43** has been subjected to intense derivatization, including P1 modification, P2-P1' exploration and P3 truncation (**Fig 13**). First, the failure of the alteration of P1 to benzimidazole (**44a-44c**) indicated a strict substituent requirement for the 1,2,3-triazole unit. In comparison, 4-phenyl-1,2,3-triazolium **44f** exhibited effective inhibition (IC_{50}=11 μM), and the unsubstituted triazole **44d** and trimethyl silyl triazole **44e** were ineffective, which demonstrated the importance of maintaining a proper aromatic ring in the P1 subpocket during optimization. Second, acetamide at the P2-P1' region was exchanged with cyclic and acyclic amide congeners to render a series of analogues with IC_{50} values below 10 μM, and the *i*-propyl **45b** and cyclobutyl **45d** amide derivatives exhibited compelling activity, with IC_{50} values less than 5 μM. Furthermore, researchers performed fragment truncation at the P3 position to minimize pharmacophores and thereby reduce the overall number of redundant groups and molecular weight, which could improve the physical and chemical properties as well as the ligand binding efficiency. As a satisfactory result, the truncated amides **46** exhibited comparable activity to the well-designed diamide counterparts **45** (**see Fig 12 for 45a-45d vs 46a-46d**). Karypidou et al. [64] prepared a novel library of fused 1,2,3-triazole[4,5-c] pyridine derivatives, and among these, **47-51** exhibited good

antiviral properties against human coronavirus 229E (**Table 3**).

Fig 13.

Table 3 Anti-coronavirus (229E) activities of 1,2,3-triazole[4,5-c] pyridine derivatives

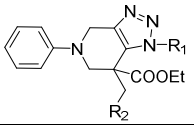

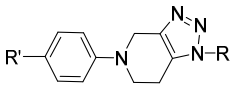

Compound	R_1	R_2	EC_{50} (μM)	Compound	R	R'	EC_{50} (μM)
47	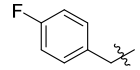	H	8.95	**50**	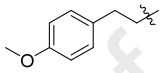	H	8.9
48	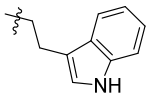	H	9.45	**51**	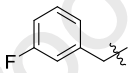	H	11.95
49	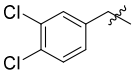	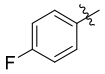	9.45				

4.3 3CL^{pro} inhibitor with a piperidine moiety

Based on an analysis of the optimization of the lead GC376 **(52)**, addition of an aldehyde bisulphite at the P1' position is necessary for the reaction with the active site Cys148 to generate tetrahedral hemithioacetal. Moreover, the γ-lactam ring at the P1 position and the Leu side chain at the P2 position should be retained and might occupy the S1 and S2 hydrophobic pockets, respectively. Additionally, extending the benzyloxy "cap" to the chlorine-substituted phenylethanol fragment yields GC813 (**53**), and its lower IC_{50} value can be attributed to an extended conformation and might orient the phenyl ring towards the hydrophobic S4 pocket. As a common privileged scaffold in drug design and discovery, the piperidine moiety is a good design element that can exhibit favourable interactions with numerous classes of proteins, which would result in optimal pharmacological activity and PK properties [65]. Thus, introducing the high-affinity piperidine moiety into the peptoid scaffold yields a series of structurally novel inhibitors (**Table 4, 54a-54f**). The piperidine-based design strategy is an effective tactic for rendering a dipeptidyl inhibitor capable of engaging in optimal binding interactions with all four S1-S4 subsites, and the resulting inhibitors have a lower molecular weight and a reduced peptidyl character compared with the tetrapeptidyl inhibitor, which is expected to display enhanced solubility and

PK lability. Gratifyingly, **54b** and **54d**, which are representative aldehyde bisulphite compounds, display potent MERS-CoV inhibitory activities with low cytotoxicity (CC_{50}>100 μM).

Table 4 Evolution of the inhibitors **54a-54f**

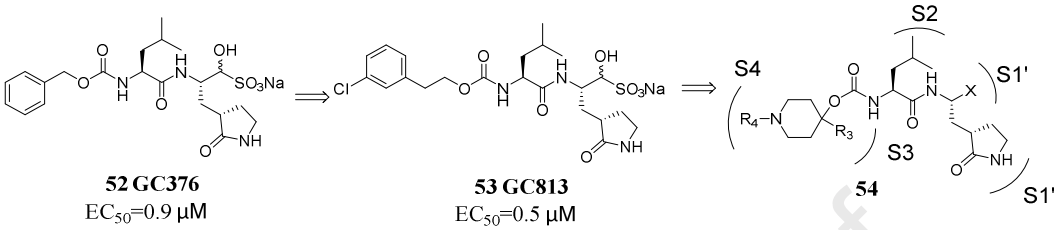

52 GC376
EC_{50}=0.9 μM

53 GC813
EC_{50}=0.5 μM

54

Compound	R_3	R_4	X	IC_{50} (μM)	
				MERS-CoV	SARS-CoV
54a	H	Boc	CHO	0.6	2.1
54b			$CH(OH)SO_3Na$	0.4	5.1
54c	$(C_6H_5)CH_2$	Boc	CHO	0.8	5.2
54d			$CH(OH)SO_3Na$	0.7	6.3
54e	H	$CH_3CH_2O(CO)$	CHO	0.6	3.2
54f			$CH(OH)SO_3Na$	0.5	8.8

4.4 Unsymmetrical aromatic disulphides

Fig 14.

Unsymmetrical aromatic disulphide compounds are a class of inhibitors that exert significant inhibitory effects on SARS $3CL^{pro}$ [66]. These new chemical entities display excellent IC_{50} values in the range of 0.516 to 5.954 μM (**Fig 14**, compounds **55-59**). Preliminary studies have indicated that these disulphides are reversible and competitive inhibitors. Among these disulphides, molecular modelling results showed that representative compound **55** binds to SARS-CoV $3CL^{pro}$ via multiple hydrogen bonds and hydrophobic contacts. Phe140, Leu141, His163, Met165, Glu166 and His172 form hydrophobic interactions with **55**, whereas Asn142, Gly143 and Cys145 form intermolecular hydrogen bonds with **55** (**Fig 15**).

Fig 15.

4.5 Serine derivatives

To develop nonpeptidic inhibitors that interact with the P1, P2 and P4 sites of $3CL^{pro}$, a new series of serine derivatives were designed by Kenichi Akaji et al. based

on the tetrapeptide aldehyde Ac-Thr-Val-Cha-His-H (**60**, IC_{50}=98 nM) and Bai's bis-cinnamoyl inhibitor (IC_{50}=10.6 μM) [67, 68]. First, imidazole, cyclohexyl, and hydroxyl groups, which were previously reported in the literature and exhibit potent biological activity, were linked to L-serine for the design of serine derivatives (**61, 62**), as shown in **Fig 16**. However, compared with peptide inhibitor **83**, these optimized groups did not provide good coverage of the substrate recognition pocket of $3CL^{pro}$ (PDB code: 3AW1), and the different binding modes of peptide inhibitors and non-peptide inhibitors with $3CL^{pro}$ led to changes in the interactions between these groups and the corresponding pocket [69]. It was hypothesized that the cyclohexyl group would occupy the S2 pocket of $3CL^{pro}$, but contrary to expectations, molecular mechanics calculations and docking simulations indicated that the cyclohexyl group of serine derivatives (**61, 62**) must occupy the S1 pocket of $3CL^{pro}$. Thus, the imidazole and hydroxyl groups of **61** and **62**, which are expected to interact with the S1 and S4 pockets, were not effective and thereby reduced the interaction between the inhibitor and $3CL^{pro}$. In addition, Bai's inhibitor **63** is located deep inside the S'1, S1 and S2 pockets and exhibits appropriate cinnamoyl functionalities [70]. Therefore, benzoyl and aniline groups were used for molecular docking with serine derivatives to obtain **64**. In addition, reasonable structural transformations of the serine derivative and hybrids constructed with other functionalities were investigated. Virtual screening using GOLD software indicated that *N*-cinnamoyl derivatives with benzoate, such as **64** and **65**, are suitable substructures.

Fig 16.

Based on the embedding of the substrate recognition pocket of the SARS $3CL^{pro}$ R188I mutant (PDB code: 3AW1), the isoserine skeleton was found to exhibit a more reasonable interaction with the mutant $3CL^{pro}$, resulting in the isoserine derivative (*R*)-**66**, which might be obtained by replacing the amine group at the α-position and adding a hydroxy group at the β-position of **65**. The docking simulation of (*R*)-**66** with SARS $3CL^{pro}$ revealed a hydrophobic space on the S2 pocket of the R188I mutant protease. Compared with hydrophobic functional groups (such as alkane, cycloalkane and aromatic rings), the phenyl group was more suitable for insertion into

the S2 pocket of the R188I mutant protease; therefore, the (2*R*,3*S*)-phenylisoserine (PIS) derivative **67** was obtained and selected as a candidate compound. An SAR study of the PIS derivative and the corresponding S1' pocket revealed that the inclusion of a cinnamic derivative (**68a, 68b**) or a phenyl propionate derivative (**68c**) at the P1' position elevated the inhibitory activity, with IC_{50} values ranging from 65 to 75 μM (**Fig 17**). In addition, cyclohexyl rings are essential to the P1 function of PIS scaffolds, whereas the cinnamyl functional group at P4 can effectively maintain the inhibitory strength.

Fig 17.

4.6 Pyrazolone and pyrimidines

Fig 18.

Based on the 1,3,4,5-tetraaryl-substituted pyrazole **69** identified through high-throughput screening, a series of 1,3,4 triple substituted pyrazolinone compounds were designed and synthesized as SARS-CoV $3CL^{pro}$ inhibitors. Among the resulting compounds (**Fig 18**), **70-73** exerted strong inhibitory effects on SARS-CoV $3CL^{pro}$, with IC_{50} values of 5.5, 10.8, 6.8 and 8.4 μM, respectively, and **73** could also effectively inhibit coxsackievirus B3 $3CL^{pro}$ [71]. Po-Huang Liang et al. further synthesized a series of analogues by grafting the neuraminidase (NA) inhibitor phenyl furan moiety into a 1,3,4 triple substituted pyrazolinone nucleus [72]. Among the resulting series, compounds **74d-74f** showed comparable inhibitory activity against SARS and MERS $3CL^{pro}$. In addition to the catalytic residue Cys145, the S1 subsite of $3CL^{pro}$ also included another important component, the oxyanion hole. This component is formed by the interaction of the C-terminal carboxylate anion of the conserved Gln with Gly143, Ser144 and Cys145, which stabilizes the transition state during proteolysis. Docking studies have indicated that the carboxylates present at the A or D ring are critical for disrupting the stability of the oxyanion hole in $3CL^{pro}$. Further SAR studies have shown that the pharmacophore phenyl at R_3 (**74a** vs**74b**) and a carboxylate at either R_1 or R_4 (**74c** vs **74d**) are essential for the activity (**Fig 18**). Because the modification of rings A and B is tolerated well, the D ring can be further altered to enhance the activity of the compounds.

Another series of 2-(benzylthio)-6-oxo-4-phenyl-1,6-dihydropyrimidines (**75a-75f**) also showed encouraging results as new anti-SARS hits [73]. The cytotoxicity of the test compounds was assessed using the MTT assay, and all the compounds were devoid of cytotoxicity. Further SAR studies revealed that compound **75c**, which has a nitro at the C-4 position, is the most potent inhibitor of SARS-CoV $3CL^{pro}$ (IC_{50}=6.1 μM). A moderately electron-withdrawing substituent at R_1, such as chloro, in compounds **75c** and **75d** improved the inhibitory activity compared with electron-donating groups, such as methyl and methoxy groups (as shown in **Table 5**). Molecular docking results have shown (docking study of **75c** with PDB code: 1UK4) that the distance between the NH of the pyrimidine ring and the oxygen atom of Glu166 was constrained by 2.0 Å. The orientation of the ligand leads to a nitrophenyl group being situated in the S1 pocket, and the nitro group points towards the surface of the protein. The oxygen of the nitro group forms hydrogen bonds with Gly143 and Cys145, and the chlorophenyl ring fits into the S2 pocket and forms hydrophobic interactions with Met49 and Gln189.

Table 5 Structure and activity of compounds **75a-75f**

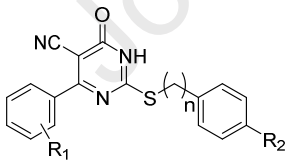

75

No	R_1	R_2	n	SARS IC_{50} (μM)
75a	4-OCH_3	4-NO_2	1	26.3
75b	4-CH_3	4-NO_2	1	>50
75c	4-Cl	4-NO_2	1	6.1
75d	4-Cl	H	2	16.9
75e	3-NO_2	4-NO_2	1	10.6
75f	3-NO_3	H	2	>50

4.7 Natural product derivatives

4.7.1 Flavonoids, biflavonoids and chalcones

Quercetin (**76**), epigallocatechin gallate (**77**) and gallocatechin gallate (**78**, GCG) also showed mild inhibitory effects against SARS-CoV $3CL^{pro}$, with IC_{50} values of 73 μM, 73 μM and 47 μM, respectively (**Fig 19**). In addition, **78** exhibited competitive inhibition towards $3CL^{pro}$, with a *K*i value of 25 μM. According to the results from a

docking analysis, the galloyl acyl moiety at the 3-OH position of compound **78,** which occupies the S1 pocket, is essential for inhibitory activity against $3CL^{pro}$ [74]. A series of inhibitors were isolated and purified from the leaves of *Torreya nucifera* (**Fig 19**). According to a preliminary screen, the biflavone amentoflavone (**79**) (IC_{50}=8.3 μM) exerted the most potent inhibitory effect against $3CL^{pro}$. An SAR study based on these flavonoids found that a methoxy substitution at the C-7 position could enhance the inhibitory effect. Specifically, the C-7 methoxy-substituted compounds **80** (IC_{50}=32.0 μM) and **81** (IC_{50} = 38.4 μM) exhibited two-fold higher inhibitory activity against SARS-CoV $3CL^{pro}$ than **82** (IC_{50}=72.3 μM) [75].

Another series of chalcones (**Fig 19**, **83-85**) isolated from *Angelica keiskei* were evaluated in terms of their anti-SARS $3CL^{pro}$ activity. Chalcone **84**, which contains perhydroxyl groups, exhibited the most potent inhibitory activity against $3CL^{pro}$, with an IC_{50} value of 11.4 μM. A detailed ligand-protein mechanistic analysis indicated that the chalcones exhibited competitive inhibition with SARS-CoV $3CL^{pro}$ [76].

4.7.2 Isatin derivatives

Previous studies have shown that isatin and its derivatives have a wide range of antiviral and antibacterial activities [77-79], including anti-HIV virus [80, 81], anti-hepatitis C virus (HCV) [82], anti-*Mycobacterium tuberculosis* and anti-pathogenic activities [83, 84]. In addition, isatin derivatives are good candidates for the development of anti-coronavirus drugs [85]. For anti-coronavirus drug discovery, a series of synthetic 5-sulphonyl isatin derivatives (**86-92**) were reported as noncovalent SARS M^{pro} inhibitors [86]. These isatin derivatives inhibited SARS-CoV $3CL^{pro}$ in the low micromolar range, and **86** (IC_{50}=1.04 μM) was found to be the most potent. SAR studies revealed that the piperidin sulphonyl-substituted compounds **86-89** exerted a more significant inhibitory effect against $3CL^{pro}$ (IC_{50}<5 μM) than the piperazine sulphonyl-substituted isatins **90-92**. Among the former, the 4-methyl piperidin sulphonyl (**87**, IC_{50}=1.18 μM) and 2-methyl piperidin sulphonyl (**88**, IC_{50}=2.25 μM) isatin derivatives were identified as the optimal candidates.

4.7.3 Terpenoid derivatives

Screening of natural products for the identification of anti-coronavirus $3CL^{pro}$

inhibitors revealed that tanshinone-type diterpenes (compounds **93-99**) derived from *Salvia miltiorrhiza* are selective inhibitors of SARS-CoV $3CL^{pro}$ and PL^{pro} [87]. With the exception of cryptotanshinone (**96**), the other isolated tanshinones exerted a dose-dependent inhibitory effect but no time-dependent effect against $3CL^{pro}$. The activity of **93-99** against $3CL^{pro}$ ranged from 14.4 to 89.1 μM. Further SAR studies revealed that subtle differences in the substituents and stereo-configuration can substantially affect the inhibitory activity. Specifically, the presence of a naphthalene moiety in the diterpene quinolone backbone appeared to improve the inhibition of $3CL^{pro}$ compared with that obtained with dimethyl-substituted tetralin (**97** and **98** vs **93** and **96**). In addition, the dihydrofuran group (**96**) on ring A of cryptotanshinone reduced the inhibitory activity by two-fold compared with that of tanshinones (**93-95**) containing a furan group.

Additionally, celastrol (**100**), pristimerin (**101**), tingenone (**102**), and iguesterin (**103**) were isolated from *Tripterygium regelii* and showed favourable competitive inhibitory activities against SARS-CoV $3CL^{pro}$, with IC_{50} values of 2.6, 9.9, 5.5 and 10.3 μM, respectively [88]. Dihydrocelastrol (**104**) was synthesized by hydrogenation with a palladium catalyst, but its $3CL^{pro}$ inhibitory activity against SARS $3CL^{pro}$ was relatively weak. Further SAR research indicated that a quinone-methide moiety in the A ring and a more hydrophobic E ring could promote inhibitory activity against $3CL^{pro}$.

Fig 19.

5. Discussion and perspectives

As the cases of SARS-CoV-2 infections continue to rise, the need for the development of effective drugs and vaccines for targeted treatment of COVID-19 is becoming increasingly urgent. Among the few available targets for anti-coronavirus drug development, $3CL^{pro}$, which is a key protein involved in the replication and transcription of coronaviruses, has become an important and relatively well-developed drug target in anti-coronavirus drug research. In addition, the SARS-CoV-2 $3CL^{pro}$ crystal structure (PDB code: 6LU7) is the first non-structural functional protein of

SARS-CoV-2 that has a confirmed conserved structure compared with those of SARS and MERS $3CL^{pro}$. Thus, broad-spectrum coronavirus $3CL^{pro}$ inhibitors are particularly suitable for the treatment of current and future coronavirus epidemics. The present article reviews the research progress on coronavirus $3CL^{pro}$ inhibitors, including synthetic peptidomimetic and nonpeptidic inhibitors and natural product derivatives, derived from various sources over the past 10 years (2010-2020) and the attempts to provide a complete description of the structural characteristics of $3CL^{pro}$ inhibitors, including details on their binding modes and other related information.

Herein, the structural characteristics, binding modes and SARs of recent coronavirus $3CL^{pro}$ inhibitors are comprehensively described. The warhead groups of peptidomimetic inhibitors mainly include aldehydes, ketones and different types of Michael receptors. These covalent irreversible inhibitors mainly utilize warhead functional groups to covalently bond with Cys145 residues in the $3CL^{pro}$ S1' pocket and thereby exert relatively durable inhibitory effects. Published studies have shown that covalent irreversible $3CL^{pro}$ inhibitors exhibit significantly improved antivirus activity, and some inhibitors can even achieve effects at nanomolar levels. However, covalent inhibitors exhibit potential off-target effects and toxic side effects. Although recent studies on peptidomimetic inhibitors are fewer than those that investigated nonpeptidic inhibitors, aldehyde compounds **11** and **12** and α-ketoamide compounds (**25-27**), which are among the recently reported peptidomimetic $3CL^{pro}$ inhibitors, exhibit excellent inhibitory activity against SARS-CoV-2. Inhibitor **11** is one of the most effective inhibitors among the aldehyde peptide series. Thus, the toxicity of inhibitor **11** over a 7-day period has been studied at different doses, specifically at dosing levels of 2, 6, and 18 mg/kg on SD rats and at a dose range of 10-40 mg/kg on beagle dogs, and all the tested animals showed significant toxicity after the inhibitor was administered once a day (QD) via intravenous drip. Therefore, **11** might be a good candidate for further clinical research on COVID-19. Coincidentally, the PK characteristics of compound **26** indicated obvious lung affinity, and this compound is suitable for administration via inhalation. Therefore, the pyridone-containing compound **26** might become another lead for further COVID-19 pandemic research.

Correspondingly, noncovalent reversible $3CL^{pro}$ inhibitors mainly exhibit weak reversible binding (such as hydrogen bonds, van der Waals forces, and hydrophobic forces) with the amino acid residues in the S1, S2, and S4 pockets, which sometimes includes the catalytically active Cys145 in the S1' pocket. This weak reversible binding could result in avoidance of the off-target risk and toxicity of irreversible inhibitors, and thus, these inhibitors might be suitable for long-term administration. Among the nonpeptidic reversible inhibitors, **55-59**, which contain a piperidine moiety, and **54a-54f**, which contain unsymmetrical aromatic disulphides, exhibit excellent inhibitory activity. Some natural products and derivatives, such as isatin [89], flavonoids, and tanshinone, might also be good candidates for the development of anti-coronavirus drugs. Specifically, **46a, 54a, 74d** and **75c** are noncovalent SARS-CoV $3CL^{pro}$ inhibitors with a moderate molecular weight and good antiviral activity and can potentially be utilized as lead templates for further drug design and screening.

However, $3CL^{pro}$ noncovalent inhibitors also have some shortcomings, such as drug effects that are not strong and/or durable, which means that these noncovalent inhibitors would need to be administered at high dosages or multiple times. Noncovalent inhibitors can also result in the emergence of resistance after long-term administration. Based on a review of the advantages and disadvantages of both covalent and noncovalent inhibitors of $3CL^{pro}$, we recommend that reversible covalent inhibitors of $3CL^{pro}$ constitute a new research direction. Specifically, the Michael warhead can be replaced by cyano (or trifluoromethyl), which might result in the formation of a reversible covalent bond with the Cys145 residue, which is unique to the coronavirus $3CL^{pro}$ S1' pocket, and this binding can potentially reduce the "off-target" risk and toxic side effects while enhancing the efficacy [90-93].

Fig 20.

Further analyses of previous studies on $3CL^{pro}$ inhibitors in association with the booming research on proteolysis-targeting chimaeras (PROTACs) [94, 95] have led to the emergence of the following drug development ideologies. PROTAC technology can be used in the design of anti-coronavirus drugs that induce the intracellular

degradation of functional nsps of exogenous viruses. The principle of PROTAC technology involves the use of a bifunctional small molecule to link the target protein and the E3 ligase in the cell such that the target protein is ubiquitinated, and the ubiquitinated protein is then recognized by the proteasome, which leads to degradation of the target protein [96]. To date, various endogenous proteins, such as BTK, PARP1, HDAC6, AR, ER, BET, BRD4, BRD9, RIPK2, TBK1, Sirt2, CDK9, p38α, pirin, c-Met, EGFR, FAK, and FLT3, have been reportedly degraded using PROTAC technology [97-99]. However, the application of PROTAC technology for the degradation of foreign proteins (such as viral proteins) remains in its infancy. To date, only the NS3/4A protease degrader DGY-08-097 of HCV has been reported, and its antiviral activity and resistance characteristics are significantly superior to those of the traditional drug telaprevir [100]. Thus, we propose that the existing $3CL^{pro}$ inhibitors can be combined with PROTAC technology to develop coronavirus $3CL^{pro}$ PROTACs. These PROTAC degraders could exhibit the advantages of both occupancy-driven $3CL^{pro}$ inhibitors and those of event-driven PROTACs: low-dose exposure would result in multiple rounds of $3CL^{pro}$ degradation and would avoid the intracellular accumulation of $3CL^{pro}$ in infected cells. These procedures would completely block the biological function of coronavirus $3CL^{pro}$ and its downstream viral proteins and would therefore inhibit the assembly and replication of the coronavirus in infected cells (shown in **Fig 20**). Reversible covalent PROTACs for $3CL^{pro}$ have been designed and synthesized in our laboratory for further screening, and we expect that these inhibitors will overcome the shortcomings of traditional $3CL^{pro}$ inhibitors and take advantage of the degradation effects of PROTACs.

Acknowledgements

This work was supported by the National Natural Science Foundation of China (grant nos. 81602967 and 81803784), the China Postdoctoral Science Foundation (grant nos. 2016M592898XB and 2019M663921XB), the Basic Research Program of Natural Science of Shaanxi Province (grant nos. 2019JQ-779, 2020CGXNG-044, 19JC006, 2019JQ-484 and 2019JQ-252), the Basic Research Plan of the Education

Department of Shaanxi Province (grant no. 19JC006), and the College Students' Innovative Entrepreneurial Training Program (grant nos. 201510708172, 201610708019, and 2019107080827).

References

[1] F. Wu, S. Zhao, B. Yu, Y. Chen, W. Wang, Z. Song, Y. Hu, Z. Tao, J. Tian, Y. Pei, A new coronavirus associated with human respiratory disease in China, Nature, 579 (2020) 265-269.

[2] J.T. Wu, K. Leung, G.M. Leung, Nowcasting and forecasting the potential domestic and international spread of the 2019-nCoV outbreak originating in Wuhan, China: a modelling study, Lancet (London, England), 395 (2020) 689-697.

[3] D.S. Hui, I.A. E, T.A. Madani, F. Ntoumi, R. Kock, O. Dar, G. Ippolito, T.D. McHugh, Z.A. Memish, C. Drosten, A. Zumla, E. Petersen, The continuing 2019-nCoV epidemic threat of novel coronaviruses to global health - The latest 2019 novel coronavirus outbreak in Wuhan, China, International journal of infectious diseases : IJID : official publication of the International Society for Infectious Diseases, 91 (2020) 264-266.

[4] J.T. Wu, K. Leung, G.M. Leung, Nowcasting and forecasting the potential domestic and international spread of the 2019-nCoV outbreak originating in Wuhan, China: a modelling study, The Lancet, 395 (2020) 689-697.

[5] J.F. Chan, S. Yuan, K.H. Kok, K.K. To, H. Chu, J. Yang, F. Xing, J. Liu, C.C. Yip, R.W. Poon, H.W. Tsoi, S.K. Lo, K.H. Chan, V.K. Poon, W.M. Chan, J.D. Ip, J.P. Cai, V.C. Cheng, H. Chen, C.K. Hui, K.Y. Yuen, A familial cluster of pneumonia associated with the 2019 novel coronavirus indicating person-to-person transmission: a study of a family cluster, Lancet (London, England), 395 (2020) 514-523.

[6] P. Zhou, X.L. Yang, X.G. Wang, B. Hu, L. Zhang, W. Zhang, H.R. Si, Y. Zhu, B. Li, C.L. Huang, H.D. Chen, J. Chen, Y. Luo, H. Guo, R.D. Jiang, M.Q. Liu, Y. Chen, X.R. Shen, X. Wang, X.S. Zheng, K. Zhao, Q.J. Chen, F. Deng, L.L. Liu, B. Yan, F.X. Zhan, Y.Y. Wang, G.F. Xiao, Z.L. Shi, A pneumonia outbreak associated with a new coronavirus of probable bat origin, Nature, 579 (2020) 270-273.

[7] C. Huang, Y. Wang, X. Li, L. Ren, J. Zhao, Y. Hu, L. Zhang, G. Fan, J. Xu, X. Gu, Clinical features of patients infected with 2019 novel coronavirus in Wuhan, China, The Lancet, 395 (2020) 497-506.

[8] J. Cui, F. Li, Z. Shi, Origin and evolution of pathogenic coronaviruses, Nature Reviews Microbiology, 17 (2019) 181-192.

[9] S. van Boheemen, M. de Graaf, C. Lauber, T.M. Bestebroer, V.S. Raj, A.M. Zaki, A.D.M.E. Osterhaus, B.L. Haagmans, A.E. Gorbalenya, E.J. Snijder, R.A.M. Fouchier, Genomic Characterization of a Newly Discovered Coronavirus Associated with Acute Respiratory Distress Syndrome in Humans, mBio, 3 (2012) e00473-00412.

[10] V. Nukoolkarn, V.S. Lee, M. Malaisree, O. Aruksakulwong, S. Hannongbua, Molecular dynamic simulations analysis of ritonavir and lopinavir as SARS-CoV 3CL(pro) inhibitors, Journal of theoretical biology, 254 (2008) 861-867.

[11] S. Skariyachan, S.B. Challapilli, S. Packirisamy, S.T. Kumargowda, V.S. Sridhar, Recent Aspects on the Pathogenesis Mechanism, Animal Models and Novel Therapeutic Interventions for Middle East Respiratory Syndrome Coronavirus Infections, Frontiers in Microbiology, 10 (2019) 569.

[12] S. Mustafa, H. Balkhy, M.N. Gabere, Current treatment options and the role of peptides as

potential therapeutic components for Middle East Respiratory Syndrome (MERS): A review, Journal of Infection and Public Health, 11 (2017) 9-17.

[13] D.S. Hui, E.I. Azhar, Y.J. Kim, Z.A. Memish, M.D. Oh, A. Zumla, Middle East respiratory syndrome coronavirus: risk factors and determinants of primary, household, and nosocomial transmission, The Lancet. Infectious diseases, 18 (2018) e217-e227.

[14] J. Cui, F. Li, Z.L. Shi, Origin and evolution of pathogenic coronaviruses, Nature reviews. Microbiology, 17 (2019) 181-192.

[15] M.A. Marra, S.J. Jones, C.R. Astell, R.A. Holt, A. Brooks-Wilson, Y.S. Butterfield, J. Khattra, J.K. Asano, S.A. Barber, S.Y. Chan, A. Cloutier, S.M. Coughlin, D. Freeman, N. Girn, O.L. Griffith, S.R. Leach, M. Mayo, H. McDonald, S.B. Montgomery, P.K. Pandoh, A.S. Petrescu, A.G. Robertson, J.E. Schein, A. Siddiqui, D.E. Smailus, J.M. Stott, G.S. Yang, F. Plummer, A. Andonov, H. Artsob, N. Bastien, K. Bernard, T.F. Booth, D. Bowness, M. Czub, M. Drebot, L. Fernando, R. Flick, M. Garbutt, M. Gray, A. Grolla, S. Jones, H. Feldmann, A. Meyers, A. Kabani, Y. Li, S. Normand, U. Stroher, G.A. Tipples, S. Tyler, R. Vogrig, D. Ward, B. Watson, R.C. Brunham, M. Krajden, M. Petric, D.M. Skowronski, C. Upton, R.L. Roper, The Genome sequence of the SARS-associated coronavirus, Science, 300 (2003) 1399-1404.

[16] Y.J. Ruan, C.L. Wei, A.L. Ee, V.B. Vega, H. Thoreau, S.T. Su, J.M. Chia, P. Ng, K.P. Chiu, L. Lim, T. Zhang, C.K. Peng, E.O. Lin, N.M. Lee, S.L. Yee, L.F. Ng, R.E. Chee, L.W. Stanton, P.M. Long, E.T. Liu, Comparative full-length genome sequence analysis of 14 SARS coronavirus isolates and common mutations associated with putative origins of infection, Lancet (London, England), 361 (2003) 1779-1785.

[17] D. Wrapp, N. Wang, K.S. Corbett, J.A. Goldsmith, C.L. Hsieh, O. Abiona, B.S. Graham, J.S. McLellan, Cryo-EM structure of the 2019-nCoV spike in the prefusion conformation, Science, 367 (2020) 1260-1263.

[18] X. Xu, P. Chen, J. Wang, J. Feng, H. Zhou, X. Li, W. Zhong, P. Hao, Evolution of the novel coronavirus from the ongoing Wuhan outbreak and modeling of its spike protein for risk of human transmission, Science China. Life sciences, 63 (2020) 457-460.

[19] Z. Jin, X. Du, Y. Xu, Y. Deng, M. Liu, Y. Zhao, B. Zhang, X. Li, L. Zhang, C. Peng, Y. Duan, J. Yu, L. Wang, K. Yang, F. Liu, R. Jiang, X. Yang, T. You, X. Liu, X. Yang, F. Bai, H. Liu, X. Liu, L.W. Guddat, W. Xu, G. Xiao, C. Qin, Z. Shi, H. Jiang, Z. Rao, H. Yang, Structure of M(pro) from SARS-CoV-2 and discovery of its inhibitors, Nature, 582 (2020) 289-293.

[20] A.A. Elfiky, Ribavirin, Remdesivir, Sofosbuvir, Galidesivir, and Tenofovir against SARS-CoV-2 RNA dependent RNA polymerase (RdRp): A molecular docking study, Life Sciences, 253 (2020) 117592-117592.

[21] C. Wu, Y. Liu, Y. Yang, P. Zhang, W. Zhong, Y. Wang, Q. Wang, Y. Xu, M. Li, X. Li, M. Zheng, L. Chen, H. Li, Analysis of therapeutic targets for SARS-CoV-2 and discovery of potential drugs by computational methods, Acta pharmaceutica Sinica. B, 10 (2020) 766-788.

[22] M. Hoffmann, H. Kleine-Weber, S. Schroeder, N. Krüger, T. Herrler, S. Erichsen, T.S. Schiergens, G. Herrler, N.H. Wu, A. Nitsche, M.A. Müller, C. Drosten, S. Pöhlmann, SARS-CoV-2 Cell Entry Depends on ACE2 and TMPRSS2 and Is Blocked by a Clinically Proven Protease Inhibitor, Cell, 181 (2020) 271-280.e278.

[23] R. Yan, Y. Zhang, Y. Li, L. Xia, Y. Guo, Q. Zhou, Structural basis for the recognition of SARS-CoV-2 by full-length human ACE2, Science, 367 (2020) 1444-1448.

[24] U. Bacha, J. Barrila, A. Velazquez-Campoy, S.A. Leavitt, E. Freire, Identification of novel

inhibitors of the SARS coronavirus main protease 3CLpro, Biochemistry, 43 (2004) 4906-4912.

[25] K. Anand, J. Ziebuhr, P. Wadhwani, J.R. Mesters, R. Hilgenfeld, Coronavirus main proteinase (3CLpro) structure: basis for design of anti-SARS drugs, Science, 300 (2003) 1763-1767.

[26] Y. Chen, Q. Liu, D. Guo, Emerging coronaviruses: Genome structure, replication, and pathogenesis, Journal of medical virology, 92 (2020) 418-423.

[27] S. Hussain, J. Pan, Y. Chen, Y. Yang, J. Xu, Y. Peng, Y. Wu, Z. Li, Y. Zhu, P. Tien, D. Guo, Identification of novel subgenomic RNAs and noncanonical transcription initiation signals of severe acute respiratory syndrome coronavirus, J Virol, 79 (2005) 5288-5295.

[28] L. Lai, X. Han, H. Chen, P. Wei, C. Huang, S. Liu, K. Fan, L. Zhou, Z. Liu, J. Pei, Y. Liu, Quaternary structure, substrate selectivity and inhibitor design for SARS 3C-like proteinase, Current pharmaceutical design, 12 (2006) 4555-4564.

[29] B. Xia, X. Kang, Activation and maturation of SARS-CoV main protease, Protein & Cell, 2 (2011) 282-290.

[30] K. Fan, L. Ma, X. Han, H. Liang, P. Wei, Y. Liu, L. Lai, The substrate specificity of SARS coronavirus 3C-like proteinase, Biochem Biophys Res Commun, 329 (2005) 934-940.

[31] H. Yang, M. Bartlam, Z. Rao, Drug design targeting the main protease, the Achilles' heel of coronaviruses, Current pharmaceutical design, 12 (2006) 4573-4590.

[32] R. Ramajayam, K.P. Tan, P.H. Liang, Recent development of 3C and 3CL protease inhibitors for anti-coronavirus and anti-picornavirus drug discovery, Biochemical Society transactions, 39 (2011) 1371-1375.

[33] M. Berry, B.C. Fielding, J. Gamieldien, Potential Broad Spectrum Inhibitors of the Coronavirus 3CLpro: A Virtual Screening and Structure-Based Drug Design Study, Viruses, 7 (2015) 6642-6660.

[34] M.F. Hsu, C.J. Kuo, K.T. Chang, H.C. Chang, C.C. Chou, T.P. Ko, H.L. Shr, G.G. Chang, A.H. Wang, P.H. Liang, Mechanism of the maturation process of SARS-CoV 3CL protease, The Journal of biological chemistry, 280 (2005) 31257-31266.

[35] K. Anand, G.J. Palm, J.R. Mesters, S.G. Siddell, J. Ziebuhr, R. Hilgenfeld, Structure of coronavirus main proteinase reveals combination of a chymotrypsin fold with an extra alpha-helical domain, The EMBO journal, 21 (2002) 3213-3224.

[36] Y. Li, J. Zhang, N. Wang, H. Li, Y. Shi, G. Guo, K. Liu, H. Zeng, Q. Zou, Therapeutic Drugs Targeting 2019-nCoV Main Protease by High-Throughput Screening, bioRxiv, (2020). Published online 28 January 2020, https://doi.org/10.1101/2020.01.28.922922.

[37] R. Lu, X. Zhao, J. Li, P. Niu, B. Yang, H. Wu, W. Wang, H. Song, B. Huang, N. Zhu, Y. Bi, X. Ma, F. Zhan, L. Wang, T. Hu, H. Zhou, Z. Hu, W. Zhou, L. Zhao, J. Chen, Y. Meng, J. Wang, Y. Lin, J. Yuan, Z. Xie, J. Ma, W.J. Liu, D. Wang, W. Xu, E.C. Holmes, G.F. Gao, G. Wu, W. Chen, W. Shi, W. Tan, Genomic characterisation and epidemiology of 2019 novel coronavirus: implications for virus origins and receptor binding, Lancet (London, England), 395 (2020) 565-574.

[38] J. He, L. Hu, X. Huang, C. Wang, Z. Zhang, Y. Wang, D. Zhang, W. Ye, Potential of coronavirus 3C-like protease inhibitors for the development of new anti-SARS-CoV-2 drugs: Insights from structures of protease and inhibitors, International journal of antimicrobial agents, (2020) 106055.

[39] Y.W. Chen, C.B. Yiu, K.Y. Wong, Prediction of the SARS-CoV-2 (2019-nCoV) 3C-like protease (3CL (pro)) structure: virtual screening reveals velpatasvir, ledipasvir, and other drug repurposing candidates, F1000Research, 9 (2020) 129.

[40] F. Wu, S. Zhao, B. Yu, Y.M. Chen, W. Wang, Z.G. Song, Y. Hu, Z.W. Tao, J.H. Tian, Y.Y. Pei, M.L. Yuan, Y.L. Zhang, F.H. Dai, Y. Liu, Q.M. Wang, J.J. Zheng, L. Xu, E.C. Holmes, Y.Z. Zhang, A new

coronavirus associated with human respiratory disease in China, Nature, 579 (2020) 265-269.

[41] P. Wei, K. Fan, H. Chen, L. Ma, C. Huang, L. Tan, D. Xi, C. Li, Y. Liu, A. Cao, L. Lai, The N-terminal octapeptide acts as a dimerization inhibitor of SARS coronavirus 3C-like proteinase, Biochem Biophys Res Commun, 339 (2006) 865-872.

[42] J. Jacobs, V. Grum-Tokars, Y. Zhou, M. Turlington, S.A. Saldanha, P. Chase, A. Eggler, E.S. Dawson, Y.M. Baez-Santos, S. Tomar, A.M. Mielech, S.C. Baker, C.W. Lindsley, P. Hodder, A. Mesecar, S.R. Stauffer, Discovery, synthesis, and structure-based optimization of a series of N-(tert-butyl)-2-(N-arylamido)-2-(pyridin-3-yl) acetamides (ML188) as potent noncovalent small molecule inhibitors of the severe acute respiratory syndrome coronavirus (SARS-CoV) 3CL protease, J Med Chem, 56 (2013) 534-546.

[43] Y. Kim, S.R. Mandadapu, W.C. Groutas, K.O. Chang, Potent inhibition of feline coronaviruses with peptidyl compounds targeting coronavirus 3C-like protease, Antiviral research, 97 (2013) 161-168.

[44] A.K. Ghosh, K. Xi, K. Ratia, B.D. Santarsiero, W. Fu, B.H. Harcourt, P.A. Rota, S.C. Baker, M.E. Johnson, A.D. Mesecar, Design and synthesis of peptidomimetic severe acute respiratory syndrome chymotrypsin-like protease inhibitors, J Med Chem, 48 (2005) 6767-6771.

[45] L. Zhu, S. George, M.F. Schmidt, S.I. Al-Gharabli, J. Rademann, R. Hilgenfeld, Peptide aldehyde inhibitors challenge the substrate specificity of the SARS-coronavirus main protease, Antiviral research, 92 (2011) 204-212.

[46] D.H. Goetz, Y. Choe, E. Hansell, Y.T. Chen, M. McDowell, C.B. Jonsson, W.R. Roush, J. McKerrow, C.S. Craik, Substrate specificity profiling and identification of a new class of inhibitor for the major protease of the SARS coronavirus, Biochemistry, 46 (2007) 8744-8752.

[47] H.Z. Zhang, H. Zhang, W. Kemnitzer, B. Tseng, J. Cinatl, Jr., M. Michaelis, H.W. Doerr, S.X. Cai, Design and synthesis of dipeptidyl glutaminyl fluoromethyl ketones as potent severe acute respiratory syndrome coronovirus (SARS-CoV) inhibitors, J Med Chem, 49 (2006) 1198-1201.

[48] M.O. Sydnes, Y. Hayashi, V.K. Sharma, T. Hamada, U. Bacha, J. Barrila, E. Freire, Y. Kiso, Synthesis of glutamic acid and glutamine peptides possessing a trifluoromethyl ketone group as SARS-CoV 3CL protease inhibitors, Tetrahedron, 62 (2006) 8601-8609.

[49] J.J. Shie, J.M. Fang, T.H. Kuo, C.J. Kuo, P.H. Liang, H.J. Huang, Y.T. Wu, J.T. Jan, Y.S. Cheng, C.H. Wong, Inhibition of the severe acute respiratory syndrome 3CL protease by peptidomimetic alpha,beta-unsaturated esters, Bioorg Med Chem, 13 (2005) 5240-5252.

[50] A.K. Ghosh, K. Xi, V. Grum-Tokars, X. Xu, K. Ratia, W. Fu, K.V. Houser, S.C. Baker, M.E. Johnson, A.D. Mesecar, Structure-based design, synthesis, and biological evaluation of peptidomimetic SARS-CoV 3CLpro inhibitors, Bioorg Med Chem Lett, 17 (2007) 5876-5880.

[51] S. Yang, S.J. Chen, M.F. Hsu, J.D. Wu, C.T. Tseng, Y.F. Liu, H.C. Chen, C.W. Kuo, C.S. Wu, L.W. Chang, W.C. Chen, S.Y. Liao, T.Y. Chang, H.H. Hung, H.L. Shr, C.Y. Liu, Y.A. Huang, L.Y. Chang, J.C. Hsu, C.J. Peters, A.H. Wang, M.C. Hsu, Synthesis, crystal structure, structure-activity relationships, and antiviral activity of a potent SARS coronavirus 3CL protease inhibitor, J Med Chem, 49 (2006) 4971-4980.

[52] Y.M. Shao, W.B. Yang, T.H. Kuo, K.C. Tsai, C.H. Lin, A.S. Yang, P.H. Liang, C.H. Wong, Design, synthesis, and evaluation of trifluoromethyl ketones as inhibitors of SARS-CoV 3CL protease, Bioorg Med Chem, 16 (2008) 4652-4660.

[53] R.P. Jain, H.I. Pettersson, J. Zhang, K.D. Aull, P.D. Fortin, C. Huitema, L.D. Eltis, J.C. Parrish, M.N. James, D.S. Wishart, J.C. Vederas, Synthesis and evaluation of keto-glutamine analogues as

potent inhibitors of severe acute respiratory syndrome 3CLpro, J Med Chem, 47 (2004) 6113-6116.

[54] P. Thanigaimalai, S. Konno, T. Yamamoto, Y. Koiwai, A. Taguchi, K. Takayama, F. Yakushiji, K. Akaji, S.E. Chen, A. Naser-Tavakolian, A. Schön, E. Freire, Y. Hayashi, Development of potent dipeptide-type SARS-CoV 3CL protease inhibitors with novel P3 scaffolds: design, synthesis, biological evaluation, and docking studies, Eur J Med Chem, 68 (2013) 372-384.

[55] P. Thanigaimalai, S. Konno, T. Yamamoto, Y. Koiwai, A. Taguchi, K. Takayama, F. Yakushiji, K. Akaji, Y. Kiso, Y. Kawasaki, S.E. Chen, A. Naser-Tavakolian, A. Schön, E. Freire, Y. Hayashi, Design, synthesis, and biological evaluation of novel dipeptide-type SARS-CoV 3CL protease inhibitors: structure-activity relationship study, Eur J Med Chem, 65 (2013) 436-447.

[56] L. Zhang, D. Lin, Y. Kusov, Y. Nian, Q. Ma, J. Wang, A. von Brunn, P. Leyssen, K. Lanko, J. Neyts, A. de Wilde, E.J. Snijder, H. Liu, R. Hilgenfeld, α-Ketoamides as Broad-Spectrum Inhibitors of Coronavirus and Enterovirus Replication: Structure-Based Design, Synthesis, and Activity Assessment, J Med Chem, 63 (2020) 4562-4578.

[57] W. Dai, B. Zhang, X.-M. Jiang, H. Su, J. Li, Y. Zhao, X. Xie, Z. Jin, J. Peng, F. Liu, C. Li, Y. Li, F. Bai, H. Wang, X. Chen, X. Cen, S. Hu, X. Yang, J. Wang, X. Liu, G. Xiao, H. Jiang, Z. Rao, L.-K. Zhang, Y. Xu, H. Yang, H. Liu, Structure-Based Design, Synthesis and Biological Evaluation of Peptidomimetic Aldehydes as a Novel Series of Antiviral Drug Candidates Targeting the SARS-CoV-2 Main Protease, bioRxiv, (2020). Published online 25 March 2020, https://doi.org/10.1101/2020.03.25.996348.

[58] L. Zhang, D. Lin, X. Sun, U. Curth, C. Drosten, L. Sauerhering, S. Becker, K. Rox, R. Hilgenfeld, Crystal structure of SARS-CoV-2 main protease provides a basis for design of improved α-ketoamide inhibitors, Science, 368 (2020) 409-412.

[59] T. Pillaiyar, M. Manickam, V. Namasivayam, Y. Hayashi, S. Jung, An Overview of Severe Acute Respiratory Syndrome–Coronavirus (SARS-CoV) 3CL Protease Inhibitors: Peptidomimetics and Small Molecule Chemotherapy, Journal of Medicinal Chemistry, 59 (2016) 6595-6628.

[60] Y. Shimamoto, Y. Hattori, K. Kobayashi, K. Teruya, A. Sanjoh, A. Nakagawa, E. Yamashita, K. Akaji, Fused-ring structure of decahydroisoquinolin as a novel scaffold for SARS 3CL protease inhibitors, Bioorganic & Medicinal Chemistry, 23 (2015) 876-890.

[61] S. Yoshizawa, Y. Hattori, K. Kobayashi, K. Akaji, Evaluation of an octahydroisochromene scaffold used as a novel SARS 3CL protease inhibitor, Bioorganic & Medicinal Chemistry, 28 (2020) 115273.

[62] K. Ohnishi, Y. Hattori, K. Kobayashi, K. Akaji, Evaluation of a non-prime site substituent and warheads combined with a decahydroisoquinolin scaffold as a SARS 3CL protease inhibitor, Bioorganic & Medicinal Chemistry, 27 (2019) 425-435.

[63] M. Turlington, A. Chun, S. Tomar, A. Eggler, V. Grum-Tokars, J. Jacobs, J.S. Daniels, E. Dawson, A. Saldanha, P. Chase, Y.M. Baez-Santos, C.W. Lindsley, P. Hodder, A.D. Mesecar, S.R. Stauffer, Discovery of N-(benzo[1,2,3]triazol-1-yl)-N-(benzyl)acetamido)phenyl) carboxamides as severe acute respiratory syndrome coronavirus (SARS-CoV) 3CLpro inhibitors: identification of ML300 and noncovalent nanomolar inhibitors with an induced-fit binding, Bioorg Med Chem Lett, 23 (2013) 6172-6177.

[64] K. Karypidou, S.R. Ribone, M.A. Quevedo, L. Persoons, C. Pannecouque, C. Helsen, F. Claessens, W. Dehaen, Synthesis, biological evaluation and molecular modeling of a novel series of fused 1,2,3-triazoles as potential anti-coronavirus agents, Bioorganic & Medicinal Chemistry Letters, 28 (2018) 3472-3476.

[65] A.C.G. Kankanamalage, Y. Kim, V.C. Damalanka, A.D. Rathnayake, A.R. Fehr, N. Mehzabeen,

K.P. Battaile, S. Lovell, G.H. Lushington, S. Perlman, K.O. Chang, W.C. Groutas, Structure-guided design of potent and permeable inhibitors of MERS coronavirus 3CL protease that utilize a piperidine moiety as a novel design element, European Journal of Medicinal Chemistry, 150 (2018) 334-346.

[66] L. Wang, B. Bao, G. Song, C. Chen, X. Zhang, W. Lu, Z. Wang, Y. Cai, S. Li, S. Fu, Discovery of unsymmetrical aromatic disulfides as novel inhibitors of SARS-CoV main protease: Chemical synthesis, biological evaluation, molecular docking and 3D-QSAR study, European Journal of Medicinal Chemistry, 137 (2017) 450-461.

[67] H. Konno, T. Onuma, I. Nitanai, M. Wakabayashi, S. Yano, K. Teruya, K. Akaji, Synthesis and evaluation of phenylisoserine derivatives for the SARS-CoV 3CL protease inhibitor, Bioorg Med Chem Lett, 27 (2017) 2746-2751.

[68] H. Konno, M. Wakabayashi, D. Takanuma, Y. Saito, K. Akaji, Design and synthesis of a series of serine derivatives as small molecule inhibitors of the SARS coronavirus 3CL protease, Bioorganic & Medicinal Chemistry, 24 (2016) 1241-1254.

[69] K. Akaji, H. Konno, H. Mitsui, K. Teruya, Y. Shimamoto, Y. Hattori, T. Ozaki, M. Kusunoki, A. Sanjoh, Structure-based design, synthesis, and evaluation of peptide-mimetic SARS 3CL protease inhibitors, J Med Chem, 54 (2011) 7962-7973.

[70] Q. Yang, L. Chen, X. He, Z. Gao, X. Shen, D. Bai, Design and synthesis of cinanserin analogs as severe acute respiratory syndrome coronavirus 3CL protease inhibitors, Chemical & Pharmaceutical Bulletin, 56 (2008) 1400-1405.

[71] R. Ramajayam, K. Tan, H. Liu, P. Liang, Synthesis and evaluation of pyrazolone compounds as SARS-coronavirus 3C-like protease inhibitors, Bioorganic & Medicinal Chemistry, 18 (2010) 7849-7854.

[72] V. Kumar, K. Tan, Y. Wang, S. Lin, P. Liang, Identification, synthesis and evaluation of SARS-CoV and MERS-CoV 3C-like protease inhibitors, Bioorganic & Medicinal Chemistry, 24 (2016) 3035-3042.

[73] R. Ramajayam, K. Tan, H. Liu, P. Liang, Synthesis, docking studies, and evaluation of pyrimidines as inhibitors of SARS-CoV 3CL protease, Bioorganic & Medicinal Chemistry Letters, 20 (2010) 3569-3572.

[74] T.T.H. Nguyen, H. Woo, H. Kang, V.D. Nguyen, Y. Kim, D.W. Kim, S. Ahn, Y. Xia, D. Kim, Flavonoid-mediated inhibition of SARS coronavirus 3C-like protease expressed in Pichia pastoris, Biotechnology Letters, 34 (2012) 831-838.

[75] Y.B. Ryu, H.J. Jeong, J.H. Kim, Y. Kim, J. Park, D. Kim, T.T.H. Naguyen, S. Park, J.S. Chang, K.H. Park, Biflavonoids from Torreya nucifera displaying SARS-CoV 3CLpro inhibition, Bioorganic & Medicinal Chemistry, 18 (2010) 7940-7947.

[76] J. Park, J. Ko, D.W. Kim, Y.M. Kim, H. Kwon, H.J. Jeong, C.Y. Kim, K.H. Park, W.S. Lee, Y.B. Ryu, Chalcones isolated from Angelica keiskei inhibit cysteine proteases of SARS-CoV, Journal of Enzyme Inhibition and Medicinal Chemistry, 31 (2016) 23-30.

[77] H. Guo, Isatin derivatives and their anti-bacterial activities, Eur J Med Chem, 164 (2019) 678-688.

[78] A.A. Farag, Synthesis and Antimicrobial Activity of 5-(morpholinosulfonyl)isatin Derivatives Incorporating a Thiazole Moiety, Drug research, 65 (2015) 373-379.

[79] A. Jarrahpour, J. Sheikh, I. Mounsi, H. Juneja, T. Hadda, Computational evaluation and experimental in vitro antibacterial, antifungal and antiviral activity of bis-Schiff bases of isatin and its derivatives, Medicinal Chemistry Research, 22 (2012) 1203-1211.

[80] R. Meleddu, S. Distinto, A. Corona, E. Tramontano, G. Bianco, C. Melis, F. Cottiglia, E. Maccioni,

Isatin thiazoline hybrids as dual inhibitors of HIV-1 reverse transcriptase, J Enzyme Inhib Med Chem, 32 (2017) 130-136.

[81] A. Corona, R. Meleddu, F. Esposito, S. Distinto, G. Bianco, T. Masaoka, E. Maccioni, L. Menéndez-Arias, S. Alcaro, S.F. Le Grice, E. Tramontano, Ribonuclease H/DNA Polymerase HIV-1 Reverse Transcriptase Dual Inhibitor: Mechanistic Studies on the Allosteric Mode of Action of Isatin-Based Compound RMNC6, PLoS One, 11 (2016) e0147225.

[82] P. Selvam, N. Murgesh, M. Chandramohan, E. De Clercq, E. Keyaerts, L. Vijgen, P. Maes, J. Neyts, M.V. Ranst, In Vitro Antiviral Activity of some Novel Isatin Derivatives against HCV and SARS-CoV Viruses, Indian journal of pharmaceutical sciences, 70 (2008) 91-94.

[83] F. Gao, H. Yang, T. Lu, Z. Chen, L. Ma, Z. Xu, P. Schaffer, G. Lu, Design, synthesis and anti-mycobacterial activity evaluation of benzofuran-isatin hybrids, Eur J Med Chem, 159 (2018) 277-281.

[84] S.B. Kumar, M. Ravinder, G. Kishore, V. Jayathirtha Rao, P. Yogeeswari, D. Sriram, Synthesis, antitubercular and anticancer activity of new Baylis-Hillman adduct-derived N-cinnamyl-substituted isatin derivatives, Medicinal chemistry research : an international journal for rapid communications on design and mechanisms of action of biologically active agents, 23 (2014) 1934-1940.

[85] L.R. Chen, Y.C. Wang, Y.W. Lin, S.Y. Chou, S.F. Chen, L.T. Liu, Y.T. Wu, C.J. Kuo, T.S. Chen, S.H. Juang, Synthesis and evaluation of isatin derivatives as effective SARS coronavirus 3CL protease inhibitors, Bioorg Med Chem Lett, 15 (2005) 3058-3062.

[86] W. Liu, H.-M. Zhu, G.-J. Niu, E.-Z. Shi, J. Chen, B. Sun, W.-Q. Chen, H.-G. Zhou, C. Yang, Synthesis, modification and docking studies of 5-sulfonyl isatin derivatives as SARS-CoV 3C-like protease inhibitors, Bioorganic & Medicinal Chemistry, 22 (2013) 292-302.

[87] J. Park, J.H. Kim, Y. Kim, H.J. Jeong, D.W. Kim, K.H. Park, H. Kwon, S. Park, W.S. Lee, Y.B. Ryu, Tanshinones as selective and slow-binding inhibitors for SARS-CoV cysteine proteases, Bioorganic & Medicinal Chemistry, 20 (2012) 5928-5935.

[88] Y.B. Ryu, S. Park, Y. Kim, J. Lee, W.D. Seo, J.S. Chang, K.H. Park, M. Rho, W.S. Lee, SARS-CoV 3CLpro inhibitory effects of quinone-methide triterpenes from Tripterygium regelii, Bioorganic & Medicinal Chemistry Letters, 20 (2010) 1873-1876.

[89] L. Zhou, Y. Liu, W. Zhang, P. Wei, C. Huang, J. Pei, Y. Yuan, L. Lai, Isatin compounds as noncovalent SARS coronavirus 3C-like protease inhibitors, Journal of medicinal chemistry, 49 (2006) 3440-3443.

[90] D. Basu, A. Richters, D. Rauh, Structure-based design and synthesis of covalent-reversible inhibitors to overcome drug resistance in EGFR, Bioorganic & medicinal chemistry, 23 (2016) 2767-2780.

[91] I.M. Serafimova, M.A. Pufall, S. Krishnan, K. Duda, M.S. Cohen, R.L. Maglathlin, J.M. McFarland, R.M. Miller, M. Frödin, J. Taunton, Reversible targeting of noncatalytic cysteines with chemically tuned electrophiles, Nature Chemical Biology, 8 (2012) 471-476.

[92] R.M. Miller, V.O. Paavilainen, S. Krishnan, I.M. Serafimova, J. Taunton, Electrophilic fragment-based design of reversible covalent kinase inhibitors, Journal of the American Chemical Society, 135 (2013) 5298-5301.

[93] S. Krishnan, R.M. Miller, B. Tian, R.D. Mullins, M.P. Jacobson, J. Taunton, Design of Reversible, Cysteine-Targeted Michael Acceptors Guided by Kinetic and Computational Analysis, Journal of the American Chemical Society, 136 (2014) 12624-12630.

[94] A.C. Lai, C.M. Crews, Induced protein degradation: an emerging drug discovery paradigm, Nature

reviews. Drug discovery, 16 (2017) 101-114.
[95] M. Schapira, M.F. Calabrese, A.N. Bullock, C.M. Crews, Targeted protein degradation: expanding the toolbox, Nature reviews. Drug discovery, 18 (2019) 949-963.
[96] X. Sun, H. Gao, Y. Yang, M. He, Y. Wu, Y. Song, Y. Tong, Y. Rao, PROTACs: great opportunities for academia and industry, Signal Transduct Target Ther, 4 (2019) 64.
[97] B.E. Smith, S.L. Wang, S. Jaime-Figueroa, A. Harbin, J. Wang, B.D. Hamman, C.M. Crews, Differential PROTAC substrate specificity dictated by orientation of recruited E3 ligase, Nat Commun, 10 (2019) 131.
[98] A. Rodriguez-Gonzalez, K. Cyrus, M. Salcius, K. Kim, C.M. Crews, R.J. Deshaies, K.M. Sakamoto, Targeting steroid hormone receptors for ubiquitination and degradation in breast and prostate cancer, Oncogene, 27 (2008) 7201-7211.
[99] M.S. Gadd, A. Testa, X. Lucas, K.H. Chan, W. Chen, D.J. Lamont, M. Zengerle, A. Ciulli, Structural basis of PROTAC cooperative recognition for selective protein degradation, Nat Chem Biol, 13 (2017) 514-521.
[100] M. de Wispelaere, G. Du, K. Donovan, T. Zhang, N. Eleuteri, J. Yuan, J. Kalabathula, R. Nowak, E. Fischer, N. Gray, P. Yang, Small molecule degraders of the hepatitis C virus protease reduce susceptibility to resistance mutations, Nature Communications, 10 (2019) 1-11.

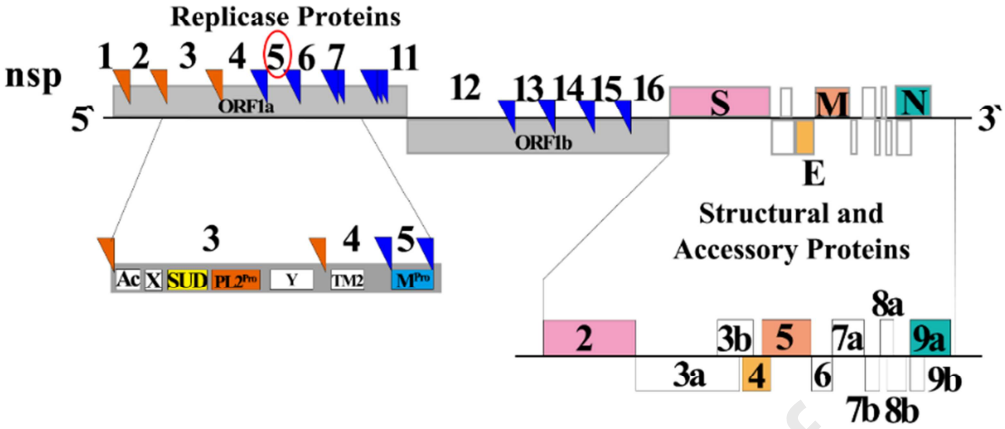

Fig 1. Coronavirus (SARS-CoV) genome.

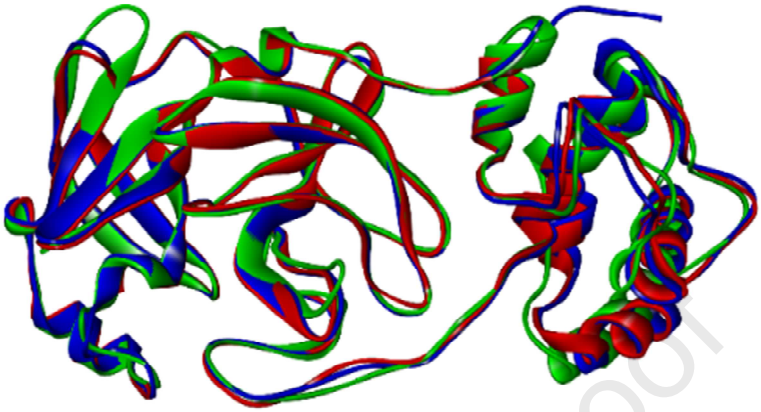

Fig 2. Simulated superposition of the structures of SARS-CoV-2 $3CL^{pro}$ (PDB code: 6LU7, blue), SARS-CoV $3CL^{pro}$ (PDB code: 1Q2W, red), and MERS-CoV $3CL^{pro}$ (PDB code: 4RSP, green).

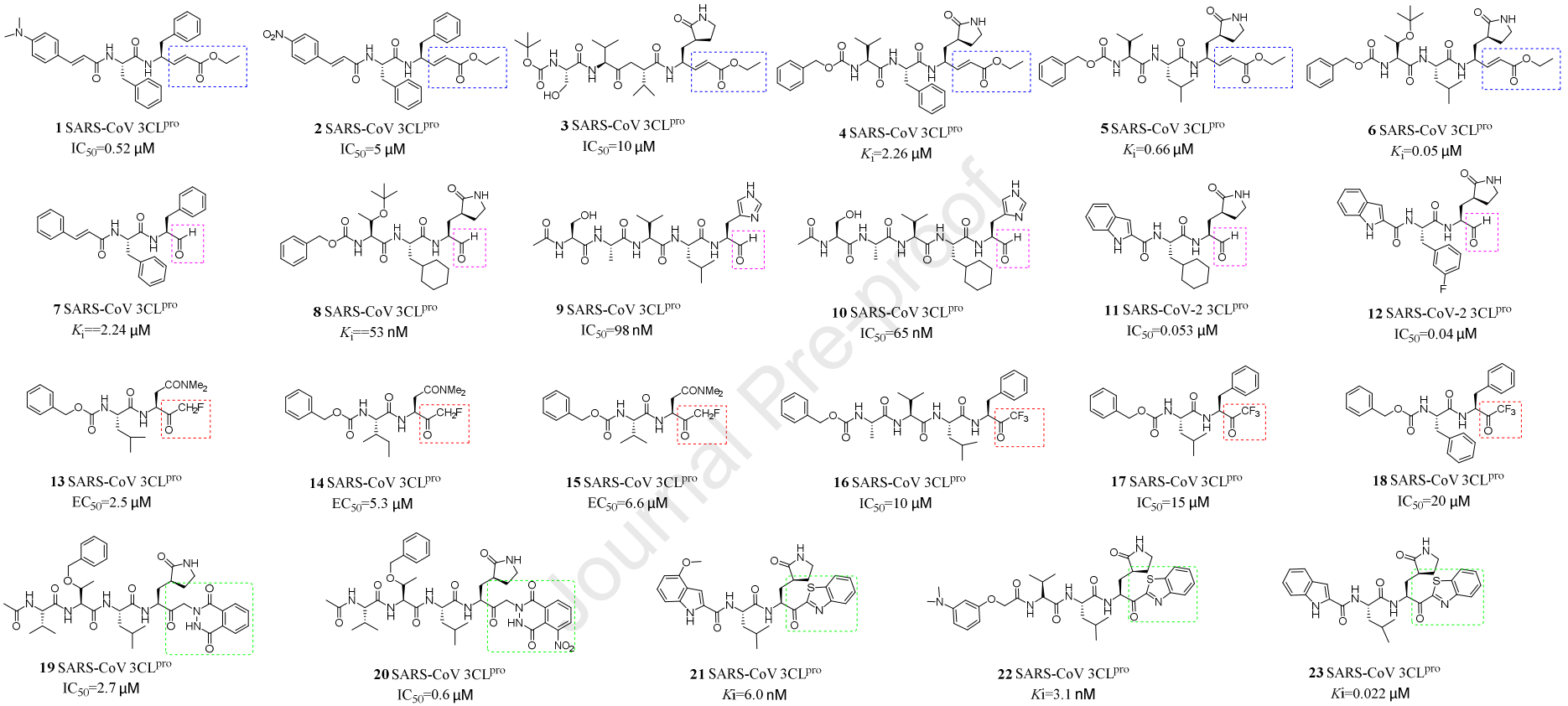

Fig 3. Peptidomimetic 3CL^{pro} inhibitors.

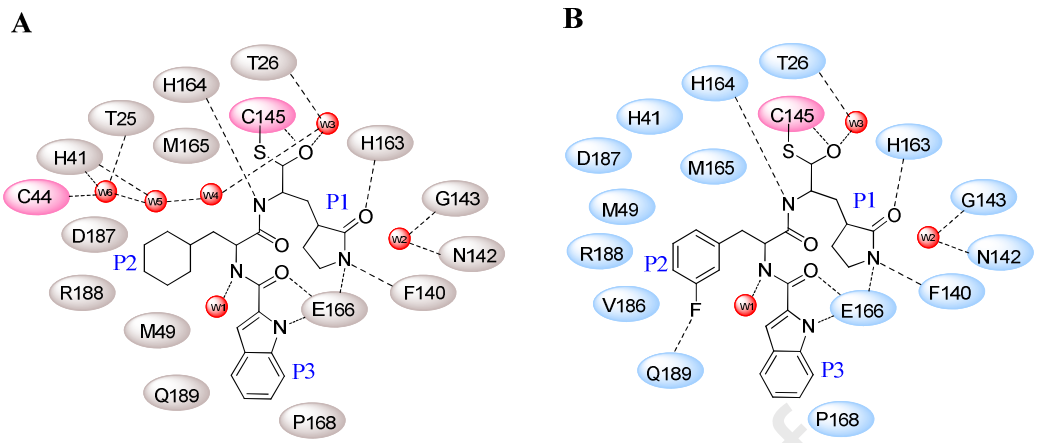

Fig 4. Schematic diagram of the X-ray crystal structure: the interaction of compounds 11 (A) and 12 (B) with SARS-CoV-2 $3CL^{pro}$.

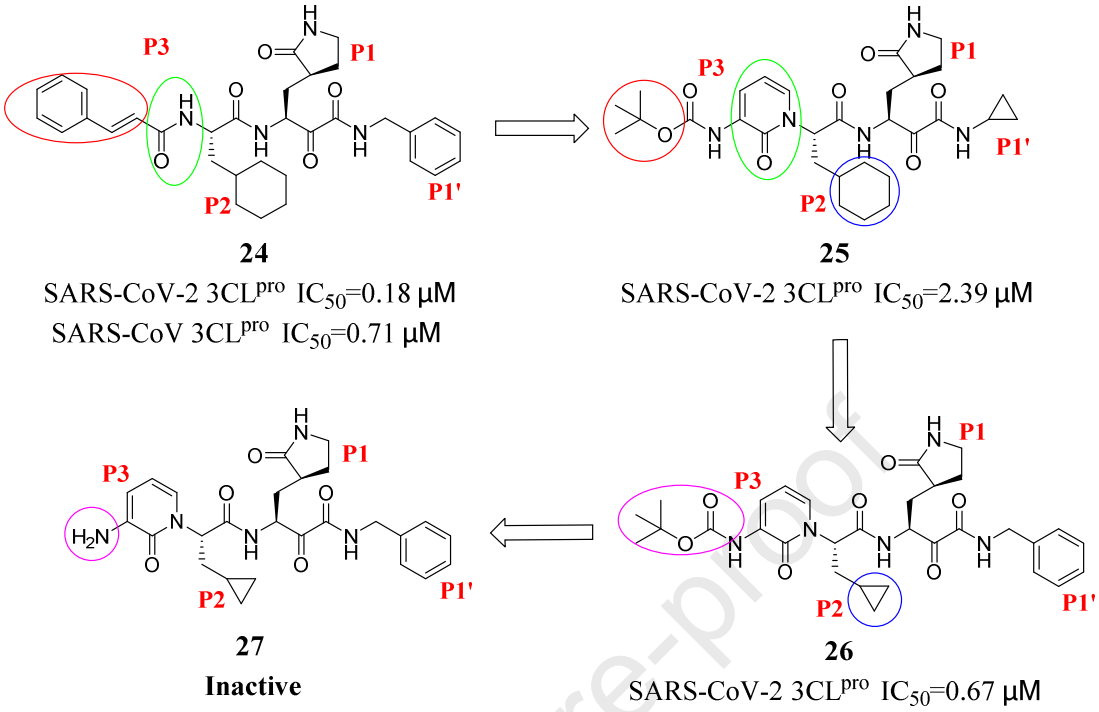

Fig 5. Chemical structures of α-ketoamide inhibitors **24**-**26**. The coloured circles highlight the specific modifications during each development step.

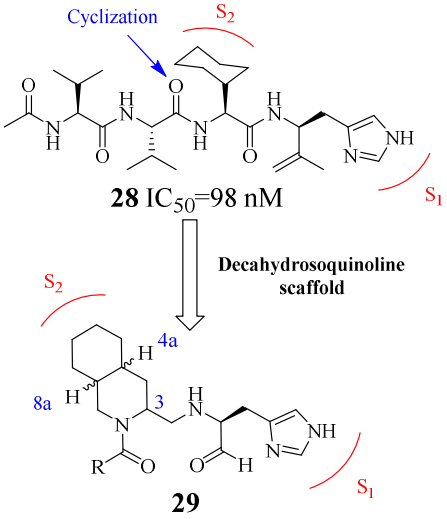

	IC_{50}	
R	**3*S*, 4a*R*, 8a*S***	**3*R*, 4a*S*, 8a*R***
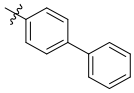	**29a** 108 μM	**29b** 240 μM
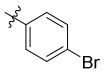	**29c** 63 μM	**29d** 175 μM

Fig 6. Novel decahydroisoquinoline derivatives that serve as SARS-CoV $3CL^{pro}$ inhibitors.

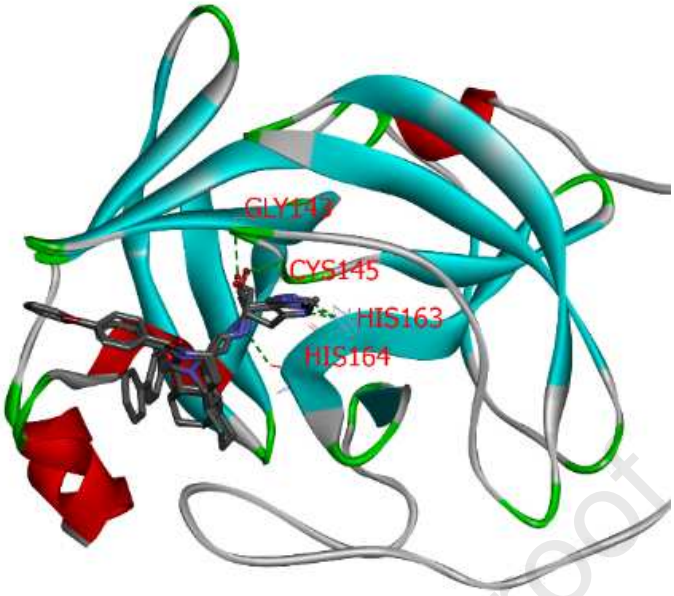

Fig 7. Crystal structure of SARS-CoV $3CL^{pro}$ superimposed with **29a**, **29b** and **29c** (PDB code: 4TWY).

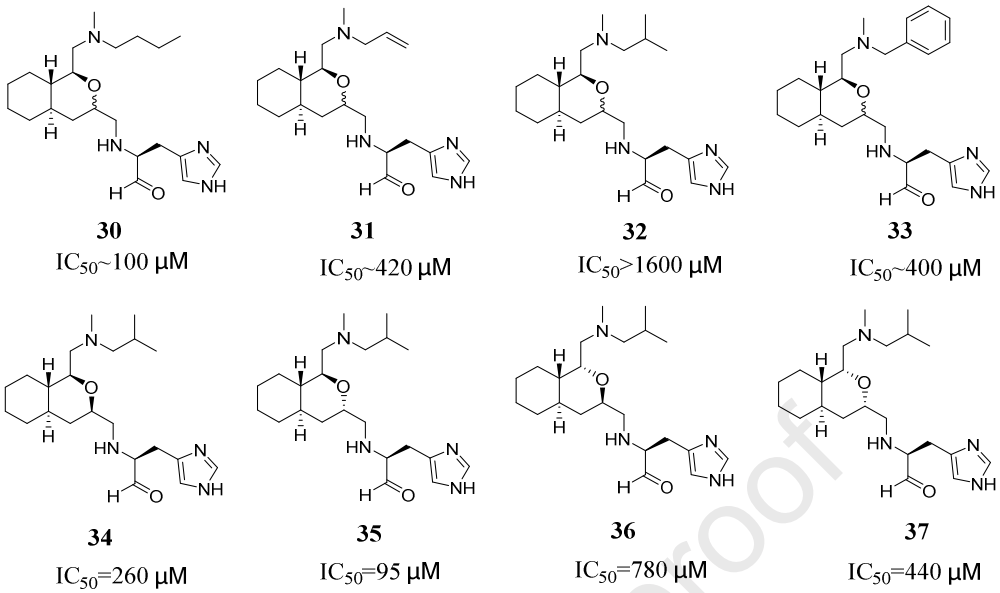

Fig 8. Octahydro-isochromene scaffold of SARS 3CL^{pro} inhibitors.

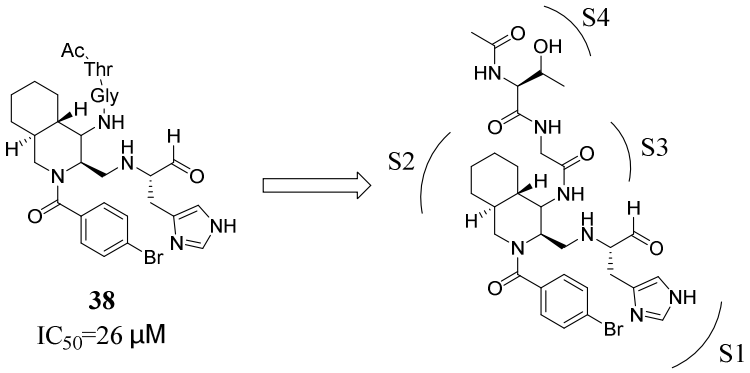

Fig 9. **38** and its binding pocket with SARS 3CL^{pro}.

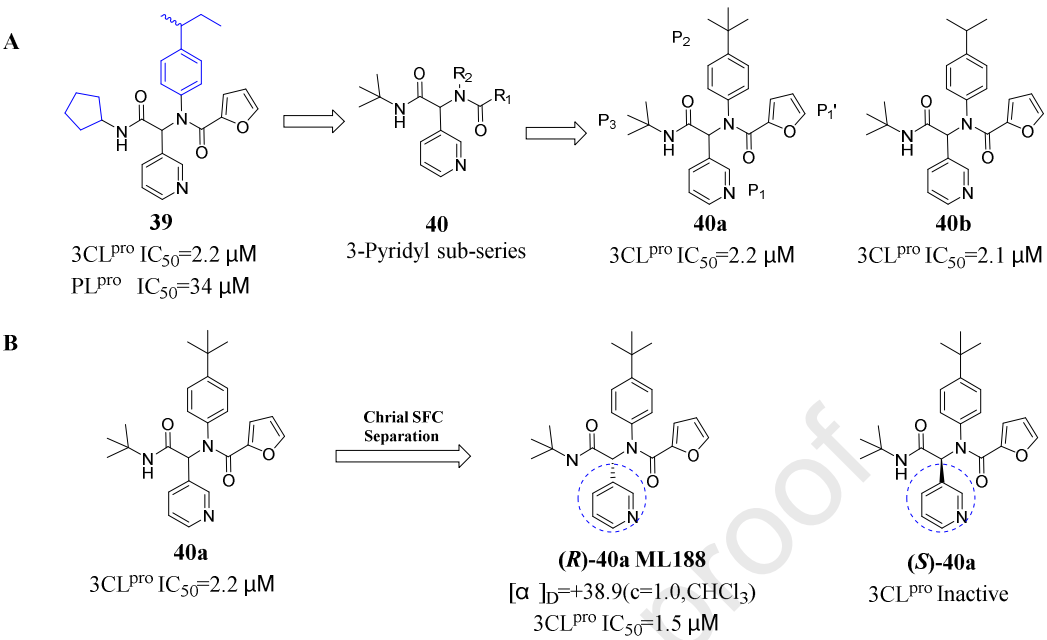

Fig 10. (A) Primary SAR study of the furyl amide hit compound **39**. (B) **(*R*)-40a** and **(*S*)-40a**.

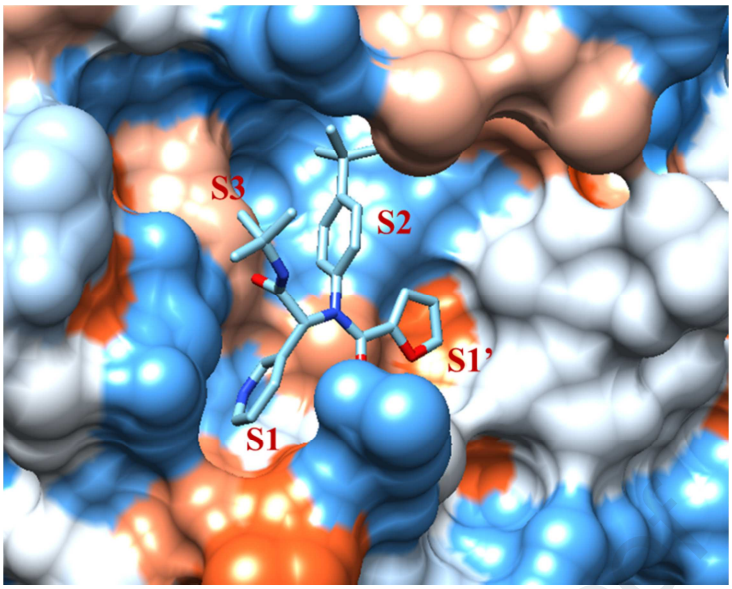

Fig 11. X-ray crystal structure of **(*R*)-40a** bound to SARS-CoV 3CL^{pro} (PDB code: 3V3M).

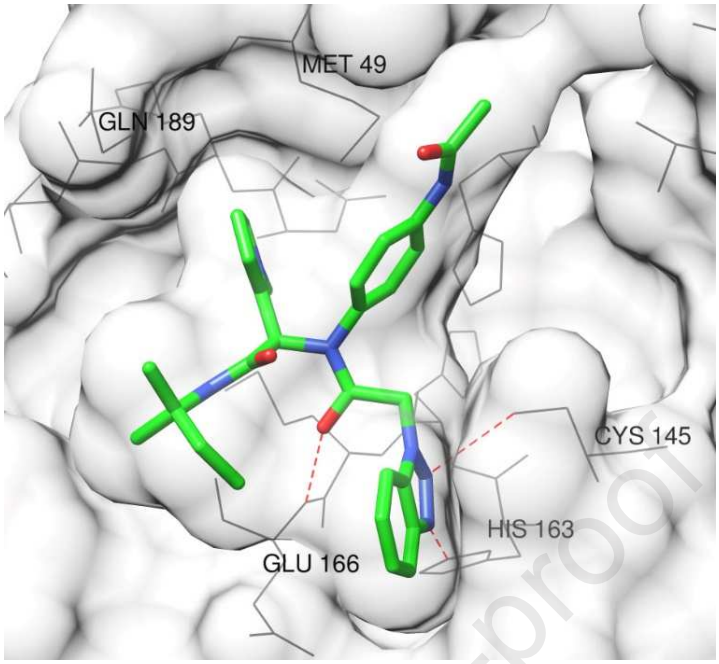

Fig 12. **43** bound to the binding pocket of SARS-CoV 3CL ^{pro} (PDB code: 4MDS).

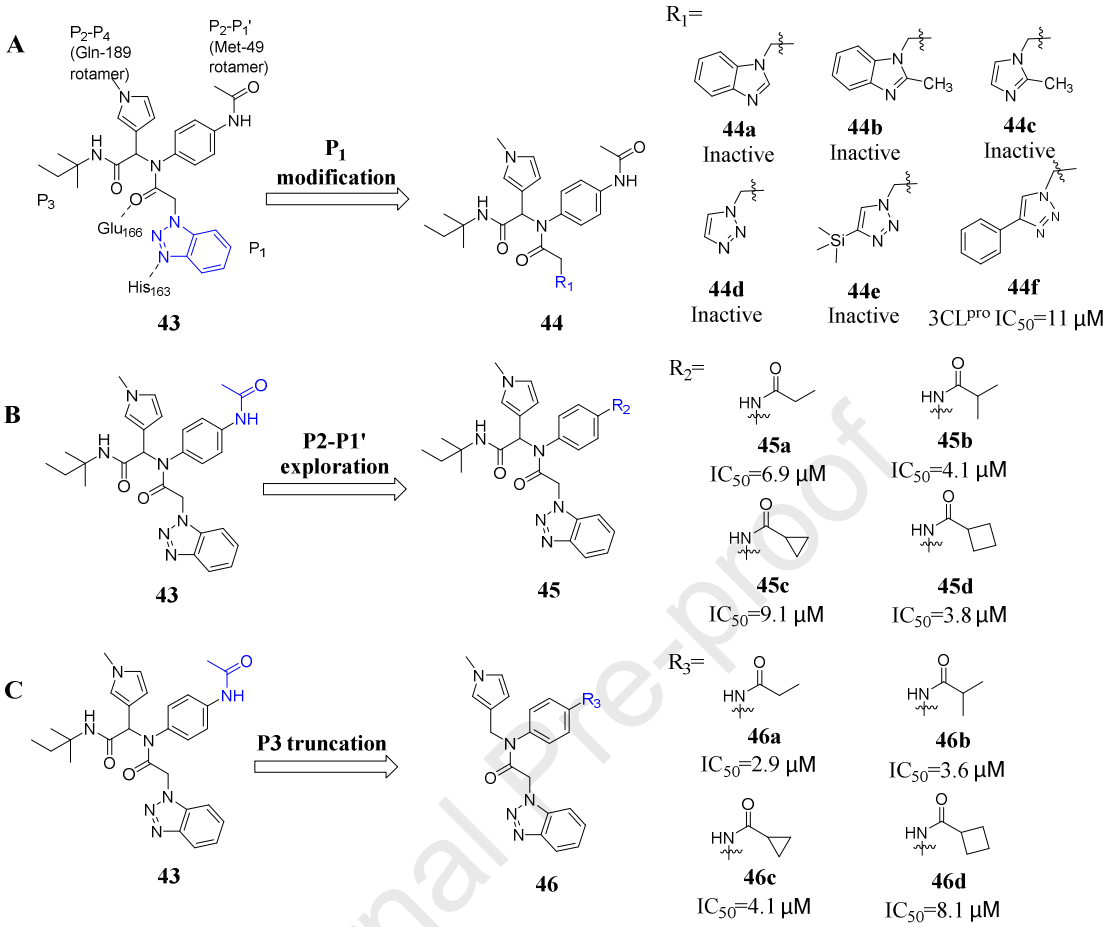

Fig 13. (A) P1 modifications, (B) P2-P1' exploration and (C) P3 truncation of the hit compound **43**.

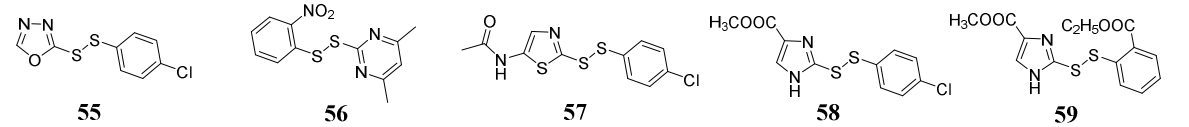

55 3CL^{pro} IC_{50}=0.516 μM

56 3CL^{pro} IC_{50}=0.921 μM

57 3CL^{pro} IC_{50}=2.262 μM

58 3CL^{pro} IC_{50}=4.126 μM

59 3CL^{pro} IC_{50}=5.954 μM

Fig 14. Unsymmetrical aromatic disulphides.

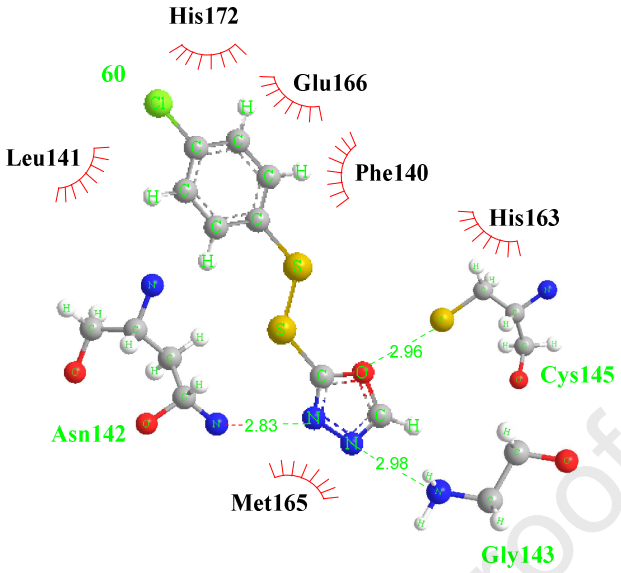

Fig 15. Modelling of **55** with SARS CoV 3CL^{pro}. The hydrogen bonds between the enzyme and the inhibitor are shown as green dashed lines, and the distances are shown in units of Å. The amino acid residues that contribute to van der Waals contacts with the inhibitor are shown as red arcs.

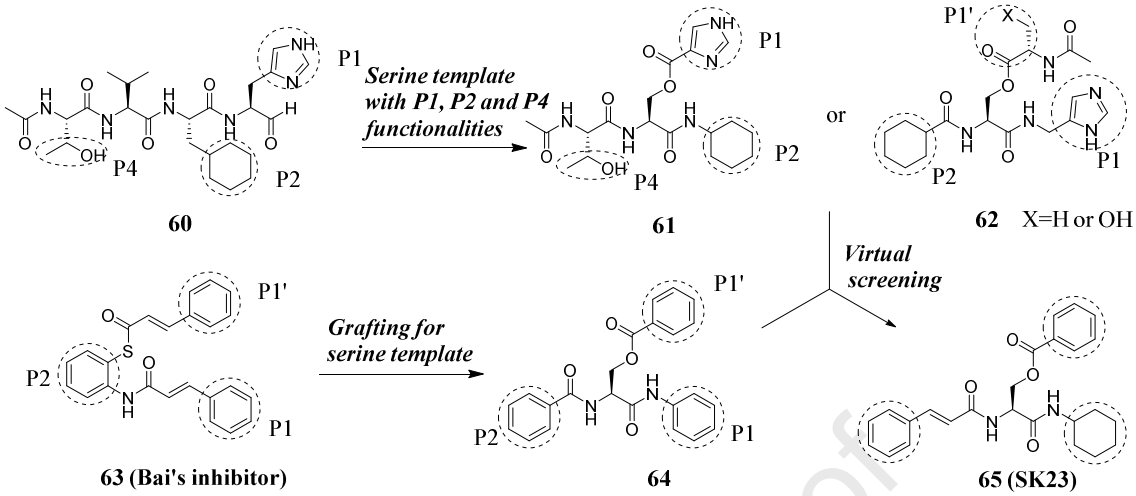

Fig 16. Design scheme of serine derivatives **64** and **65**.

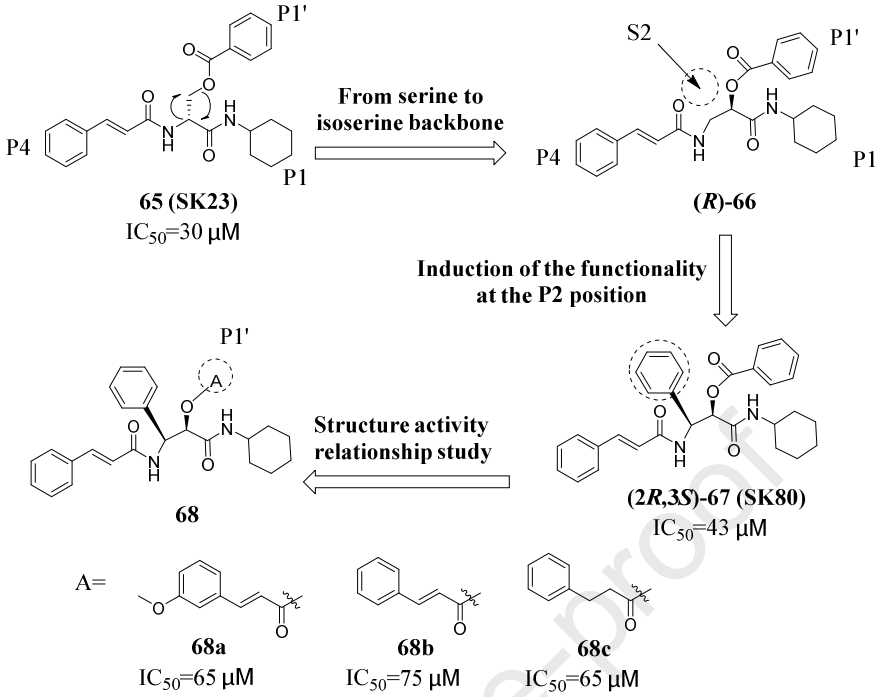

Fig 17. Evolution of phenyl isoserine derivatives **68a, 68b, and 68c** from serine derivatives.

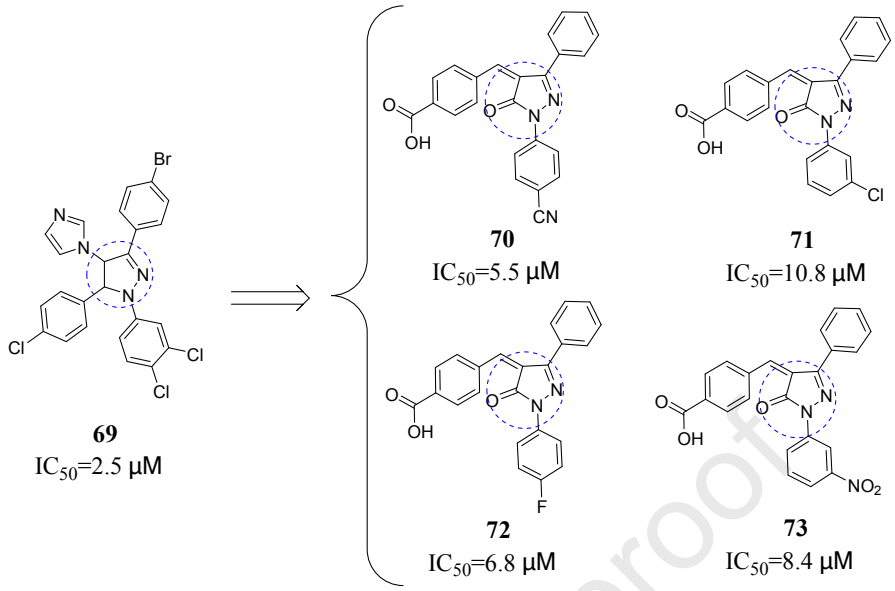

69
IC_{50}=2.5 μM

70
IC_{50}=5.5 μM

71
IC_{50}=10.8 μM

72
IC_{50}=6.8 μM

73
IC_{50}=8.4 μM

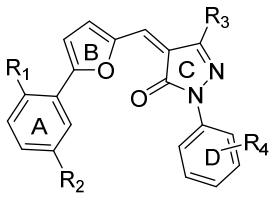

74

No	R_1	R_2	R_3	R_4	SASR IC_{50} (μM)	MERS IC_{50} (μM)
74a	COOH	Cl	CH3	H	**>** 50	**>** 50
74b	COOH	Cl	Ph	H	16.4	12.2
74c	H	H	Ph	H	**>** 50	**>** 50
74d	H	H	Ph	COOH	6.4	5.8
74e	COOH	Cl	Ph	4-$CH(CH_3)_2$	6.0	7.3
74f	COOH	Cl	Ph	4-$CH(CH_3)_3$	5.8	7.4

Fig 18. Structure of pyrazolones and their inhibition of SARS and MERS $3CL^{pro}$.

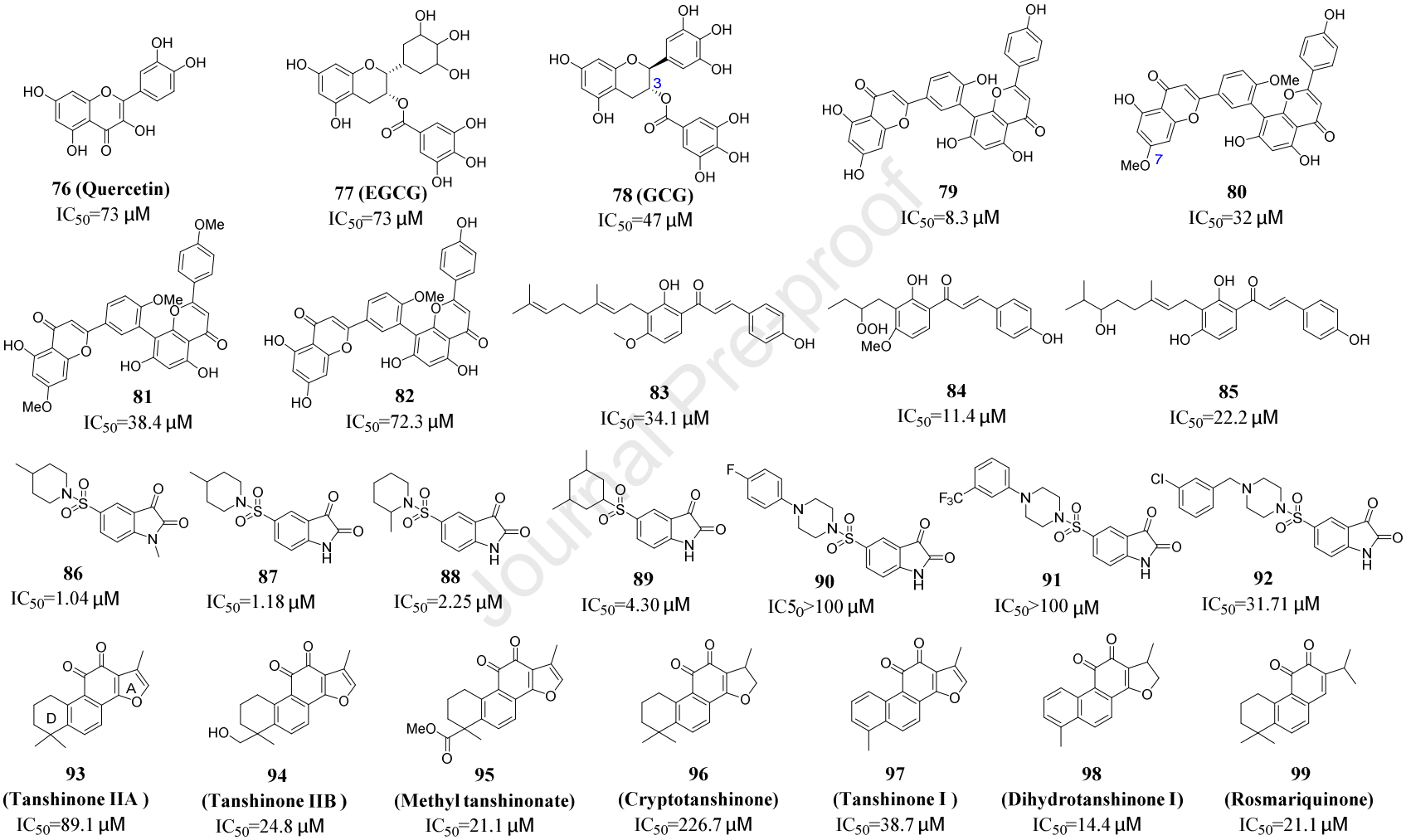

Fig 19. Chemical structures of natural product derivatives **76-110**.

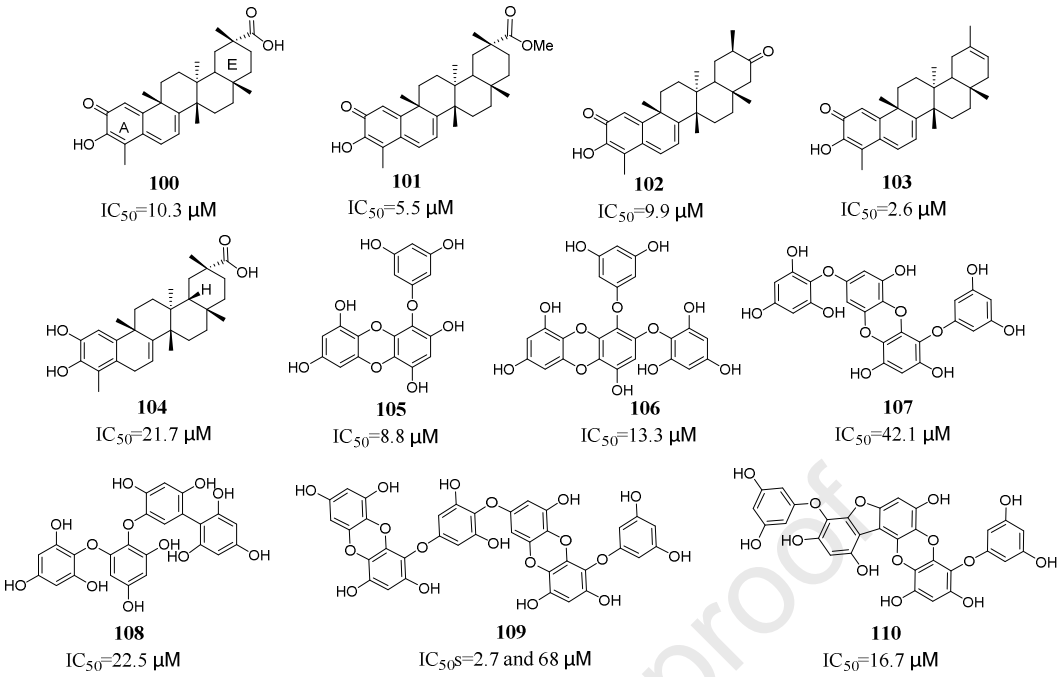

Fig 19. *Continued*.

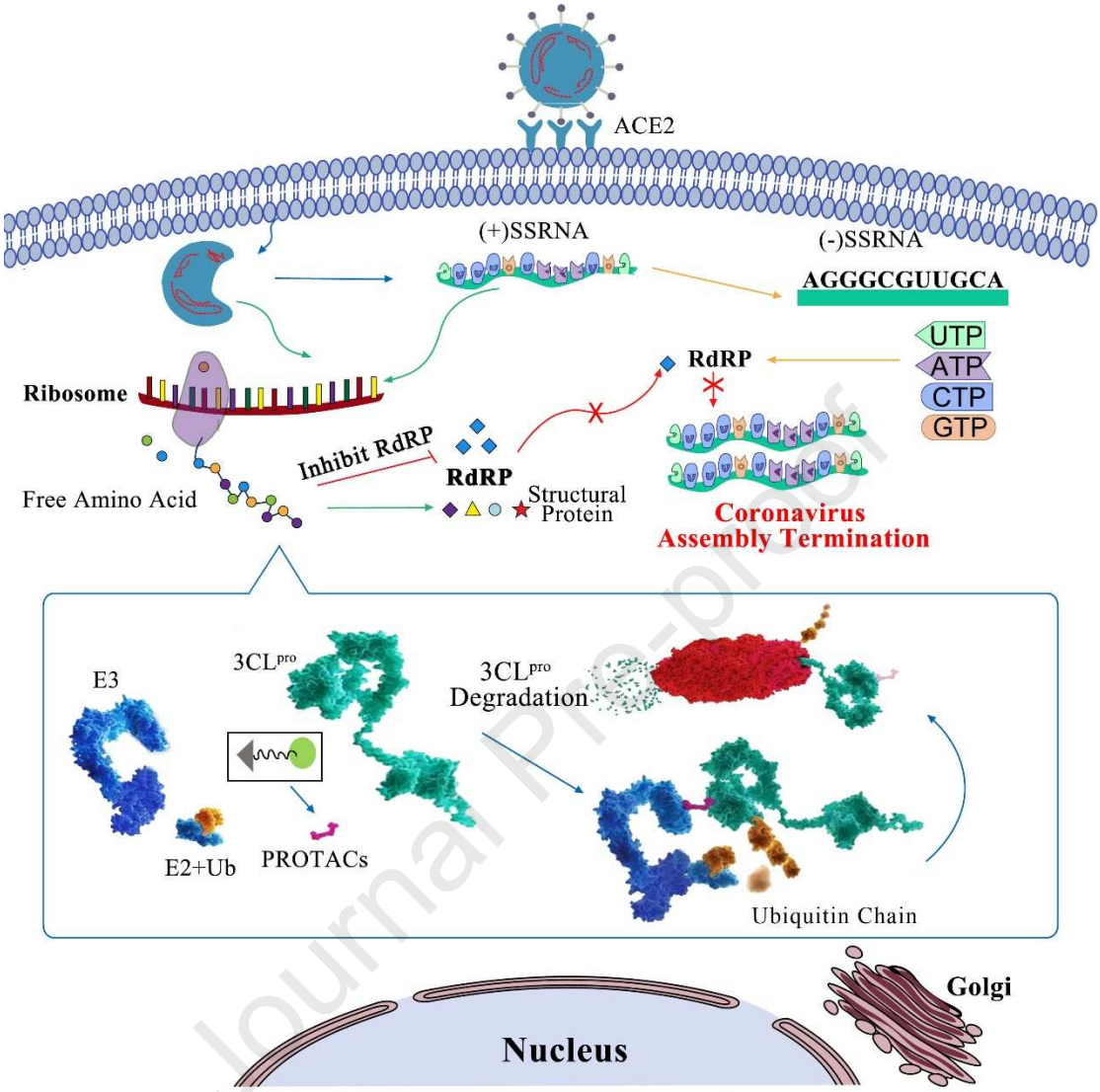

Fig 20. Illustration of PROTACs targeting the degradation of $3CL^{pro}$ and thereby inhibiting coronavirus assembly and replication.

Highlights

1. This article provides a comprehensive overview of the coronavirus $3CL^{pro}$ inhibitors developed from 2010 to 2020.
2. The SARs, structural characteristics and binding modes of peptidomimetic and nonpeptidic inhibitors are comprehensively analysed and summarized.
3. As anti-coronavirus candidates, reversible covalent PROTACs for $3CL^{pro}$ could induce the intracellular degradation of $3CL^{pro}$.

Conflict of Interest

The authors declared that they have no conflicts of interest to this work.

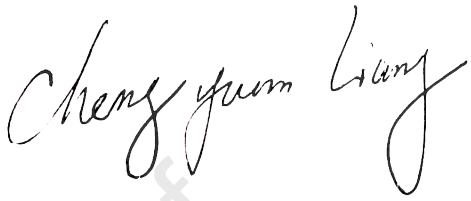

Abbreviation Index

Abbreviation	Terminology
ACE2	Angiotensin-converting enzyme 2
$3CL^{pro}$	3C-like Protease
E	Envelope protein
EUA	Emergency use authorization
FDA	The U.S. Food and Drug Administration
GCG	Gallocatechin gallate
HCV	Hepatitis C virus
His-al	(*S*)-2-amino-3-imidazolyl propanal
HIV	Human immunodeficiency virus
HCoV	human coronavirus
M	Membrane protein
MERS-CoV	Middle East respiratory syndrome coronavirus
MLPCN	Molecular Libraries Probe Production Centers Network
M^{pro}	Main protease
N	Nucleocapsid phosphoprotein
NA	Neuraminidase
NIH	National Institutes of Health
nsps	Non-structural proteins
ORF	Open reading frames
PL^{pro}	Papain-like protease
PK	pharmacokinetic
PROTAC	Proteolysis-targeting chimaera
QD	Once a day
RdRp	RNA-dependent RNA polymerase
S	Spike protein
SAR	Structure-activity relationship
SARS-CoV	Severe acute respiratory syndrome coronavirus
SARS-CoV-2	Severe acute respiratory syndrome coronavirus 2
SFC	Supercritical fluid chromatography
SPR	Surface plasmon resonance